GENERATION OF HIGH HARMONICS IN ARGON, HYDROGEN AND THEIR MIXTURES WITH NEON

A Thesis

by

MUHAMMED SAYRAÇ

Submitted to the Office of Graduate Studies of
Texas A&M University
in partial fulfillment of the requirements for the degree of

MASTER OF SCIENCE

Chair of Committee,	Hans A. Schuessler
Co-Chair of Committee,	Alexandre A. Kolomenski
Committee Member,	Dong H. Son
Head of Department,	George R. Welsh

August 2013

Major Subject: Physics

ABSTRACT

Femtosecond time scale allows us to follow and control atomic and molecular motion. The atomic vibrations happen in the range of femtosecond scale. Thus, femtosecond technology effectively measures the atomic vibration. However, to determine electron motion, one needs to reach sub-femtosecond time scale that is in attosecond time scale.

High Harmonic Generation (HHG) is a non-linear process that converts infrared light to shortest wavelength, such as in the XUV regime. HHG allows to explore electronic motion and to control electron dynamics. HHG easily reaches to XUV region and is enabling attosecond pulse generation.

In this thesis we focused to generate attosecond pulses by using noble gases and their mixtures. We used only argon gas, only hydrogen molecule and their mixture with neon gas. We wanted to improve the conversion efficiency (10^{-6}) of the fundamental light into high harmonics. We use Ne and H_2 gas mixture to look enhancement of the HHs.

DEDICATION

This dissertation is dedicated to my wife Habibe Sayraç and daughter Zeynep Beril Sayraç.

ACKNOWLEDGEMENTS

I would like to thank my committee chair, Dr. Hans A. Schuessler, my co-chair, Dr. Alexandre A. Kolomenski, and my committee member, Dr. Dong H. Son, for their guidance and support throughout the course of this research. Also I am grateful to Dr. Alexandre A. Kolomenski for helping me and for explaining how to work with the HHG setup.

I would also like to express my appreciation to all of the wonderful people who have worked in this lab over the years: Dr. James Strohaber, Necati Kaya, Gamze Kaya, and Nathan Hart. It has been a pleasure to share the lab with you.

Thanks also go to the department faculty and staff for making my time at Texas A&M University a great experience. I also want to extend my gratitude to the National Science Foundation, Welch Foundation, Qatar Foundation, Multidisciplinary University Research Initiative (MURI), and Turkish Ministry of Education.

Finally, thanks to my mother, father, my wife, and to my daughter for their encouragement during this work, especially my wife Habibe Sayrac for her patience and love.

NOMENCLATURE

as	Attosecond
CCD	Charged Coupled Device
fs	Femtosecond
HHG	High Harmonic Generation
MCP	Micro Channel Plate
SLM	Spatial Light Modulator
t	Time
XUV	Extremely Ultra Violet

TABLE OF CONTENTS

Page

LIST OF FIGURES

Page

1 INTRODUCTION

The study of light-matter interactions was started with the discovery of the photoelectric effect by Heinrich Hertz in 1887 and with studying of hydrogen emission lines (Balmer lines) by Johann Balmer in 1885. After Einstein studied the photoelectric effect in 1905, and Bohr introduced a quantum model of atom in 1913, Bohr then reproduced the Balmer's spectral line series. The understanding of emission and absorption of atoms and molecules brought science a better knowledge of the nature of light. This knowledge of the atoms and molecules resulted in the development of quantum mechanics at the beginning of the 20th century [**1**].

After the invention by Mairman of a ruby laser in 1960, intense laser fields with intensities ranging from 10^{13} $W/_{cm^2}$ to 10^{16} $W/_{cm^2}$ have started to be used in laboratories all over the world. In quantum mechanics, particles can pass through classically forbidden regions by tunneling through the barrier. When to the Coulomb potential of an atom is strongly distorted by the laser field, an electron from outer shell of the atom can tunnel from the bound state to the continuum (Keldysh 1965), and such laser fields are called strong fields [**2**]. Pulsed lasers exist that can produce short pulses with durations from nanoseconds (1 ns=10^{-9} s) to femtoseconds (1 fs=10^{-15} s). In the latter case, lasers commonly use a wavelength of around 800 nm. If electrons experience a strong interaction with the laser field they ionize, acquire kinetic energy in the laser field and then recombine with parent ions; the whole process results in large number of laser photons converted into one photon with frequency equal to a multiple of the laser

frequency. This can take place for many atoms interacting with laser field, and this process is called high harmonic generation (HHG) [**1**].

Laser radiation-matter interaction is not only an interesting subject in its own right, but is also related to a broad range of fields, for instance for tracing chemical reactions, since an ultra-short (femtosecond) pulse can be used for detection of molecular vibrations. The HHG is also used to create attosecond pulses (1 as=$10^{-18}\ s$) [**3**]. With attosecond pulses one can detect electron dynamics, which is much faster than the molecular motion [**4**]. Moreover, the HHG can be used to determine intermolecular distance [**5**], [**6**] or photo recombination cross section [**7**].

2 INTERACTION OF INTENSE LASER PULSES WITH ATOMIC AND MOLECULAR SYSTEM

2.1 The Laser Field

The classical electromagnetic field is described by the electric $\boldsymbol{E}$ and the magnetic $\boldsymbol{B}$ field vectors. These fields satisfy the Maxwell's Equations [**8**], [**9**]. The electric field and the magnetic field are derived from scalar (Φ) and vector ($\boldsymbol{A}$) potentials.

$$\boldsymbol{E}(\boldsymbol{r},\boldsymbol{t}) = -\boldsymbol{\nabla}\boldsymbol{\Phi}(\boldsymbol{r},\boldsymbol{t}) - \frac{\boldsymbol{\partial}}{\boldsymbol{\partial t}}\boldsymbol{A}(\boldsymbol{r},\boldsymbol{t}) \quad (1)$$

$$\boldsymbol{B}(\boldsymbol{r},\boldsymbol{t}) = \boldsymbol{\nabla} \times \boldsymbol{A}(\boldsymbol{r},\boldsymbol{t}) \quad (2)$$

Electric and magnetic fields are invariant under the gauge transformation because Φ and $\boldsymbol{A}$ potentials are not exactly defined according to Eq. 1 and Eq. 2. $\boldsymbol{A} \rightarrow \boldsymbol{A} + \boldsymbol{\nabla}k$, $\Phi \rightarrow \Phi - \frac{\partial}{\partial t}k$, where k is a real function depends on r and t. One can choose the vector potential.

$$\boldsymbol{\nabla} \cdot \boldsymbol{A}(\boldsymbol{r},\boldsymbol{t}) = \boldsymbol{0} \quad (3)$$

If the $\boldsymbol{A}$ satisfies condition in Eq. 3, we are in the Coulomb gauge. This choice is possible when there is not any source. Then one can take $\Phi = 0$ and $\boldsymbol{A}$ satisfies the wave equation.

$$\boldsymbol{\nabla^2}\,\boldsymbol{A}(\boldsymbol{r},\boldsymbol{t}) - \frac{\boldsymbol{1}}{\boldsymbol{c^2}}\frac{\boldsymbol{\partial^2}}{\boldsymbol{\partial t^2}}\,\boldsymbol{A}(\boldsymbol{r},\boldsymbol{t}) = \boldsymbol{0} \quad (4)$$

where c is the velocity of the light in vacuum;

The solution is written for a monochromatic field

$$\boldsymbol{A(r,t) = e\frac{E_0}{\omega_0}\sin(\omega_0 t - k.r + \varphi)} \quad (5)$$

$$\boldsymbol{E(r,t) = eE_0\cos(\omega_0 t - k.r + \varphi)} \quad (6)$$

$$\boldsymbol{B(r,t) = k \times e\frac{E_0}{\omega_0}\cos(\omega_0 t - k.r + \varphi)} \quad (7)$$

where k is the wave vector that is the propagation direction of the electromagnetic field, $\omega_0 = kc$ is the angular frequency, and φ is the phase of the laser field.

The electric field of the one atomic unit is given by $E_0 = \frac{e}{4\pi\epsilon_0 a_0^2} = 5.14x10^9\ \frac{V}{cm}$ where e is the electric charge, a_0 is the Bohr radius and ϵ_0 is the vacuum permittivity. Then the intensity of the one atomic unit is the time averaged Poynting vector (the rate of energy transfer per unit area) $I_0 = \frac{(E_0)^2}{2\mu_0 c} = 3.51x10^{16}\ \frac{W}{cm^2}$, where μ_0 is the vacuum permeability. This determines the relationship between electric field and the intensity in the atomic unit [**1**] :

$$\boldsymbol{E_0 = \sqrt{\frac{I\left(W/_{cm^2}\right)}{3.51x10^{16}}}} \quad (8)$$

2.1.1 Generating Femtosecond Pulses

Since the laser was invented in 1960, lasers have been used as a high power light source. Lasers can produce high power with low pulse energy with duration time of <100 fs, but their energy decreases with repetition rate. The pulse energy of low repetition rate femtosecond lasers can be in the order of 1 J, whereas the pulse energy is in the order of mJ for most kHz lasers. Ti:Sapphire is a commonly used gain medium for femtosecond lasers since it has a wavelength of approximately 800 nm. Femtosecond oscillators using gain medium (Ti:Sapphire) can reach pulses with milijoule-level energies, but direct amplification of the pulse to millijoule level can cause a damage to the laser crystal. To avoid the damage, the pulses from the oscillator are stretched to hundreds of picoseconds to have a lower peak power. Then the pulses need to be amplified by using a regenerative amplifier that is similar to a laser oscillator so that the pulses with high energies reach the femtosecond duration [**10**].

2.2 Ionization

Ionization is a transfer of an electron through a continuum from a bound state of an atom. Rare gases are generally used in HHG to generate attosecond pulses because they can withstand high laser intensity [**10**]. Then the electron turns back the ground level and it emits its kinetic energy as a XUV light. There are several basic requirements for femtosecond lasers to produce the attosecond pulses. First, the intensity on the gas target must be around $\sim 10^{13}\ {}^{W}/_{cm^2}$ to ionize rare gases, and the pulse energy must also be ≥100 μJ to reach required intensity. The second, the pulse duration should be short enough (<100 fs) for generating single attosecond pulses.

Hollow-core fibers filled with noble gases are suitable for broadening the spectrum of laser pulses with higher energies because the ionization potentials of noble gases are much larger than that of solids. By using solid materials, there is also a limit because the fiber can be damaged by the intense laser field. However, gases can recover after the ionization when the laser pulses are gone, but using solid materials can be permanently damaged by the laser [**10**]. For these reason, gas-filled hollow-core fibers are commonly used for attosecond pulse generation.

Ionization occurs because when the strong laser field tunnel ionizes the gas target they create an electron wave packet that is driven back and forth by the laser field. When the driven electron wave packet recombines the core, it emits an attosecond pulse [**11**].

3 THEORETICAL DESCRIPTION OF HHG

3.1 Three Step Model

High harmonic generation stems from electron-ion interactions. That means there is a probability for an electron to return to the parent atom with a high kinetic energy for each laser cycle. At the highest intensities, the bound electrons tunnel into the continuum over the Coulomb barrier. Then HHs decrease in low intensity, but then we observed a plateau where the intensity of the HHs remains approximately same. The plateau ends up with a sharp decrease called high harmonic cutoff where high harmonic generation ends, Fig. 1. The cutoff energy depends on linearly on the increasing laser intensity [**12**]. The cutoff energy also depends on the ponderomotive energy that refers to free electrons averaged kinetic energy gained in the laser electric field [**13**]. In the HHG process, when the gas atoms or molecules are driven by the intense laser field of frequency ω_1, they emit radiation of higher frequencies $q\omega_1$ where q is odd integer in Fig .2.

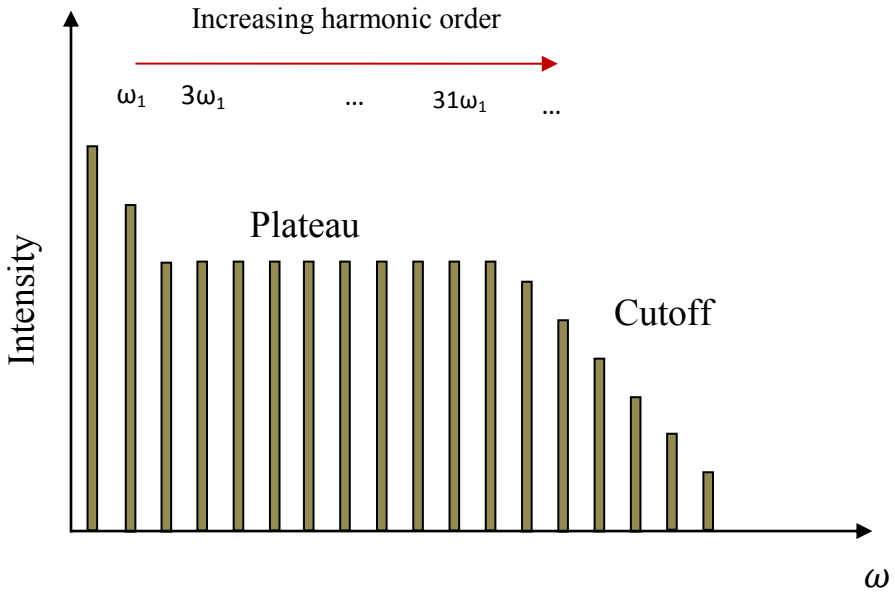

Figure 1 High Harmonic Spectra where spacing between the harmonics is regular and odd multiplier of the driving laser frequency $\boldsymbol{\omega_1}$

The cutoff ($E_{cutoff} = hv_{max}$) is given as [**14**], [**15**].

$$\mathbf{E_{cutoff} = I_p + 3.17U_p} \tag{9}$$

where $U_p = {}^{I}/_{4\omega^2}$ a.u is the ponderomotive energy, I is the laser intensity, ω is the frequency, and the I_P is the atomic ionization potential of considered atom. This shows that harmonics are mostly generated with the highest frequency and the shortest wavelengths.

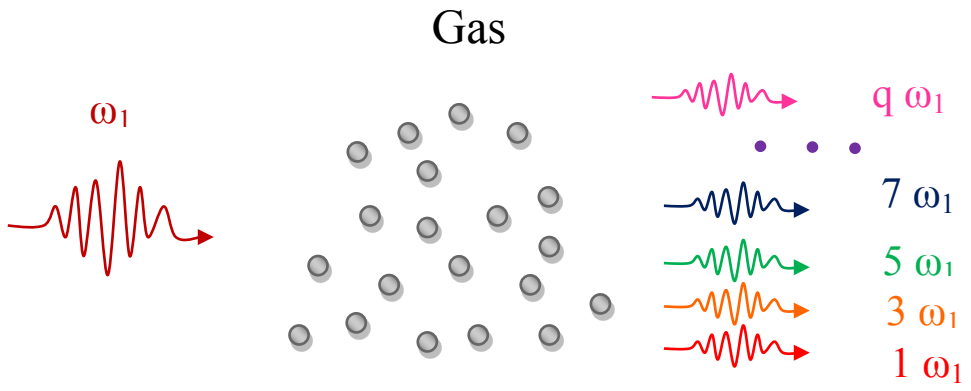

Figure 2 High Harmonic Generation (HHG) Process

The high harmonic generation has been explained by the three-step model in Fig.3 [**16**]. Initially, the electrons are confined by the coulomb potential of the nucleus. The laser electric field lowers the potential barrier at each optical half cycle. When the intensity is high enough, electrons can tunnel through the barrier, and go into the continuum. This is the first step. During the continuum, the Coulomb potential is ignored and the electrons are considered as classical particles. The laser field accelerates the electrons away from the parent ion and drives back when the electric field sign is changed. During this process, the electrons will gain larger kinetic energy from the laser electric field. This is the step two. In the step three, the electrons recombine the parent ion, and emit their kinetic energy as $3.17U_p$ [**13**], [**17**].

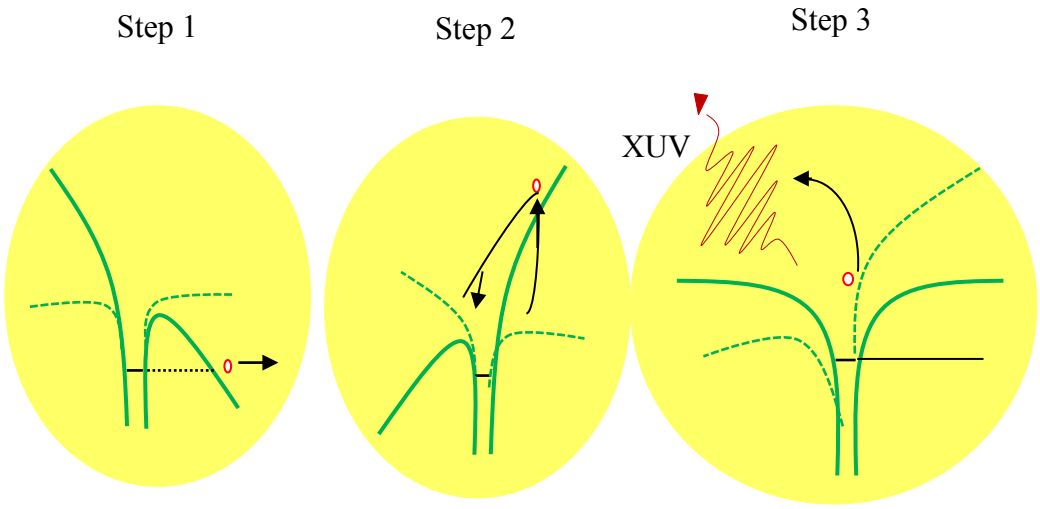

Figure 3 Three Step Model of HHG

Taking into account linearly polarized laser electric field in the z direction is given

$$\boldsymbol{E(t) = E_0 \cos \omega_0 t} \tag{10}$$

where E_0 and ω_0 are the laser field's amplitude and the frequency, respectively. If the electron is initially considered at $z(t) = 0$ position and the $\dot{z}(t) = 0$, we will have the position of the electron with the initial conditions as

$$\boldsymbol{E_{kin} = \frac{E_0^2}{2\omega_0^2}(\sin\theta - \sin\theta_i)^2 = 2U_p(\sin\theta - \sin\theta_i)^2} \tag{11}$$

$$\boldsymbol{z(t) = \frac{E_0}{\omega_0^2}[(\cos\theta - \cos\theta_i) + (\theta - \theta_i)\sin\theta_i]} \tag{12}$$

where the $\theta = \omega_0 t$ is the phase. We also obtain the kinetic energy is $E_{kin} = \frac{1}{2}\dot{z}^2$ in a.u and we get

where $U_p = \frac{E_0^2}{4\omega_0^2}$ in atomic unit. Then the emitted photon energy is given by

$$\mathbf{E_{cut} = E_{kin} + I_p} \tag{13}$$

In Eq. 13 the electron is recombined if the ionization phase is between $0 < \theta_i < \frac{\pi}{2}$, and it never returns back if $\frac{\pi}{2} < \theta_i < \pi$. E_{kin} has the maximum value at $\theta_i = 17°$ and $\theta_r = 255°$, $E_{kin} = 3.17U_p$ and then the cutoff energy is found by $\mathrm{E_{cutoff}} = \mathrm{I_p} + 3.17\mathrm{U_p}$.

One can determine the phase of ionization θ_i and the phase of recombination θ_r if knowing the E_{kin}.

$$[(\mathbf{\cos\theta_r - \cos\theta_i}) + (\boldsymbol{\theta_r - \theta_i})\,\mathbf{\sin\theta_i}] = \mathbf{0} \tag{14}$$

$$(\mathbf{\sin\theta_r - \sin\theta_i})^2 = \frac{\boldsymbol{E_{kin}}}{\mathbf{2U_p}} \tag{15}$$

The trajectory is the path of the electron from θ_i to θ_r. There are two trajectories below the $E_{kin} = 3.17U_p$ in Fig. 4. They are that the short trajectory is for $17° < \theta_i < 90°$, $90° < \theta_r < 255°$ and the long trajectory is for $0° < \theta_i < 17°, 255° < \theta_r < 360°$.

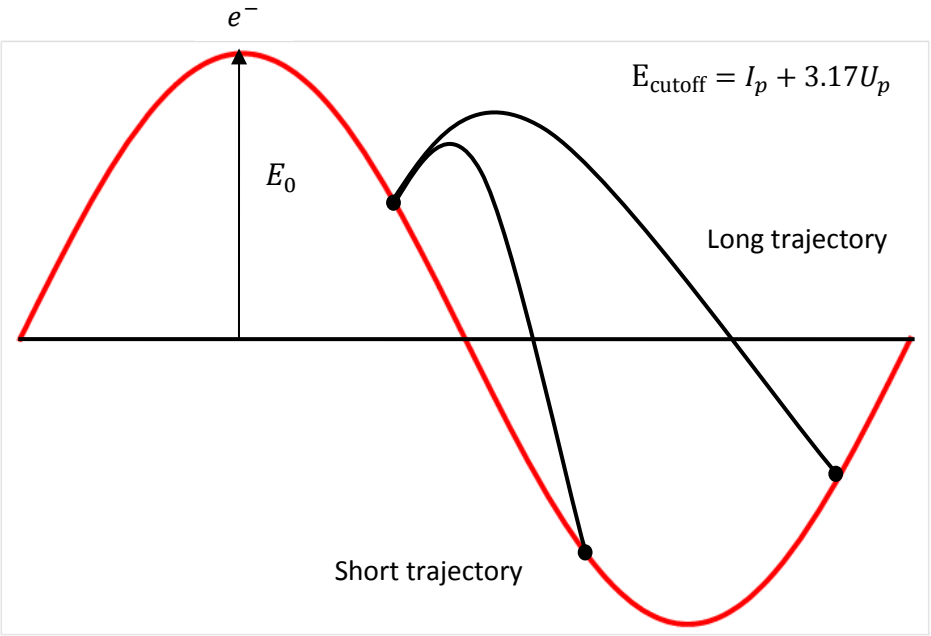

Figure 4 Behavior of the electron in oscillating field

The high harmonics are emitted each half cycle of the laser fields and the harmonic fields $E_h(t)$ can be expressed as

$$\boldsymbol{E_h(t) = \cdots + F_h\left(t + \frac{2\pi}{\omega_0}\right) - F_h\left(t + \frac{\pi}{\omega_0}\right) + F_h(t) - F_h\left(t - \frac{\pi}{\omega_0}\right) + F_h\left(t - \frac{2\pi}{\omega_0}\right) - \cdots} \quad (16)$$

The Eq.16 can take nonzero values only at odd multiplies of ω_0 that explains why we only see the odd harmonics [**16**].

High harmonics are kind of train of the pulse repeated every half cycle of the laser field of the fundamental wave as shown in Fig. 5 [**18**].

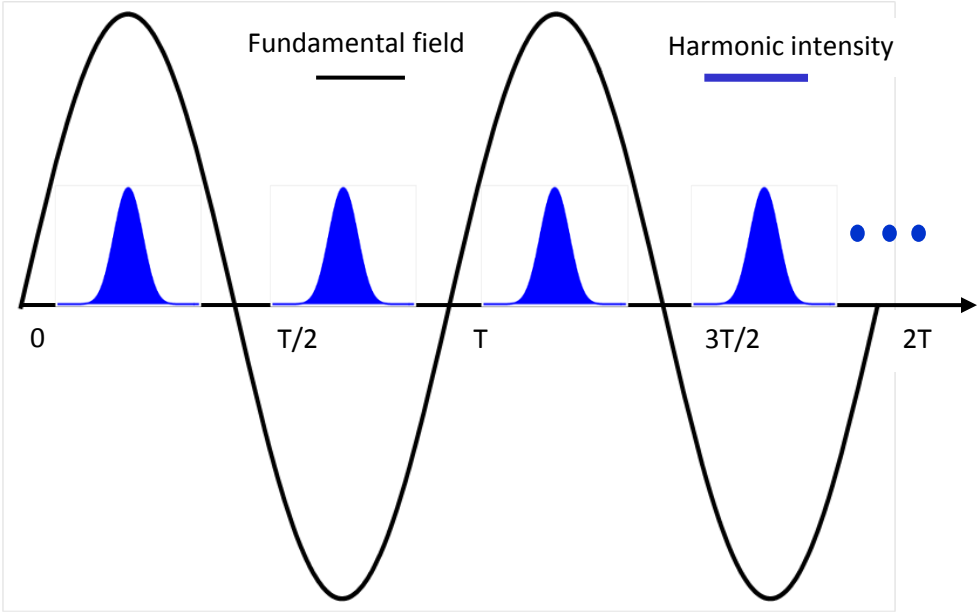

Figure 5 Bursts of HH radiation during two cycles of the fundamental optical field.

3.2 Lewenstein's Model

HHG is theoretically explained by Lewenstein's model that gives quantum-mechanical justification of the 3 step model that is classical explanation of the HHG [**19**] **,** [**16**]**.** The interaction of the laser field is described by the time-dependent Schrödinger equation (TDSE)

$$\boldsymbol{i}\frac{\boldsymbol{\partial}}{\boldsymbol{\partial t}}\Psi(\boldsymbol{r},\boldsymbol{t}) = \left[\frac{\boldsymbol{-1}}{\boldsymbol{2}}\boldsymbol{\nabla^2} + \ \boldsymbol{V}(\boldsymbol{r}) + \boldsymbol{zE}(\boldsymbol{t})\right]\Psi(\boldsymbol{r},\boldsymbol{t}) \qquad (17)$$

where $V(r)$ is the atomic potential and $E(t)$ is linearly polarized laser field in the z direction. To solve TDSE, there is an assumption called strong field approximation, the SFA model [**19**].

- The contribution of all the excited states can be neglected
- The depletion of the ground state can be neglected

- The role of the atomic potential $V(r)$ on the motion of the continuum electron can be neglected.

Under this approximation, the time-dependent dipole moment $\mu(t) = \langle \Psi(r,t)|ex|\Psi(r,t)\rangle$ is given by,

$$\boldsymbol{\mu(t) = \int_{-\infty}^{t} dt' \int d^3p d^*\big(p + A(t)\big) Exp[-iS(p,t,t')] E(t') d\big(p + A(t')\big) + c.c} \quad (18)$$

where p is the canonical momentum and d(p) is the dipole transition matrix element. $A(t) = \int E(t)dt$ is the vector potential and $S(p,t,t')$ is the semi-classical action, which means that the $S(p,t,t')$ describes the free electron motion in the laser field with a constant momentum and electron leaves from the parent atom at time t' and returns back the same position at time t, defined as

$$\boldsymbol{S(p,t,t') = \int_{t'}^{t} dt'' \left(\frac{[p + A(t'')]^2}{2} + I_p \right)} \quad (19)$$

The approximation for the hydrogen atom,

$$\boldsymbol{d(p) = -\frac{i8\sqrt{2}(2I_p)^{5/4}}{\pi} \frac{p}{(p^2 + I_p)^3}} \quad (20)$$

Also the ground state wave function is alternatively given

$$\Psi(\boldsymbol{r}) = \left((\pi \Delta^2)^{-3/4} \right) Exp \left[\frac{-r^2}{(2\Delta^2)} \right] \quad (21)$$

where $\Delta \approx \frac{1}{I_p}$ is the spatial width.

Eq. 18 is consistent with the three step model, $E(t')d\left(\boldsymbol{p}+\boldsymbol{A}(t')\right)$ corresponds to the ionization at time t', and $Exp[-iS(\boldsymbol{p},t,t')]$ gives the propagation from t' to t and $d^{*}\left(\boldsymbol{p}+\boldsymbol{A}(t)\right)$ describes the recombination at time t [**16**].

4 EXPERIMENTAL SETUP AND CONDITIONS FOR HHG

4.1 Laser Systems

Our laser system consists of four lasers feeding each other. They are named by the manufacturer as Millenia V, Kapteyn-Murnane (KM oscillator), Evolution and Spitfire (regenerative amplifier) [**20**], [**21**].

4.1.1 Millenia V

The Millennia V is a solid-state, high power, visible continuous wave (CW) laser that supplies larger than 5 W of green 1064 nm output pulse from the output of a diode pumped intracavity Nd: YAG laser. The emission is then frequency doubled by a temperature tuned lithium triborate (LBO) crystal resulting in radiation at 532 nm. In our system, Millennia V is used to pump the femtosecond oscillator Kapteyn-Murnane (KM) with a continuous optical power of 5.5 W at 532 nm wavelength [**22**].

4.1.2 Kapteyn-Murnane (KM) Oscillator

KM is a mode-locked Ti:Sapphire femtosecond oscillator pumped by Millennia V. To achieve the Kerr lens effect, concave mirrors are placed which form the telescope with the crystal in the focal plane. In Fig. 6 Ti:Sapphire femtosecond oscillator is shown where M1, M2, M3, M4, M5 are the cavity mirrors, and where M3 is also the output mirror. The group velocity dispersion experienced by the laser pulse traveling inside the crystal is compensated by a pair of prisms P1 and P2 that are also used to compensate the dispersion in the crystal. The output of the oscillator is a train of pulses emitting from

780 nm to 830 nm, pulse duration is about 35 fs, repetition rate close to 80 MHz, pulse energy 5 nJ/pulse and the average power is about 400 mW [**20**].

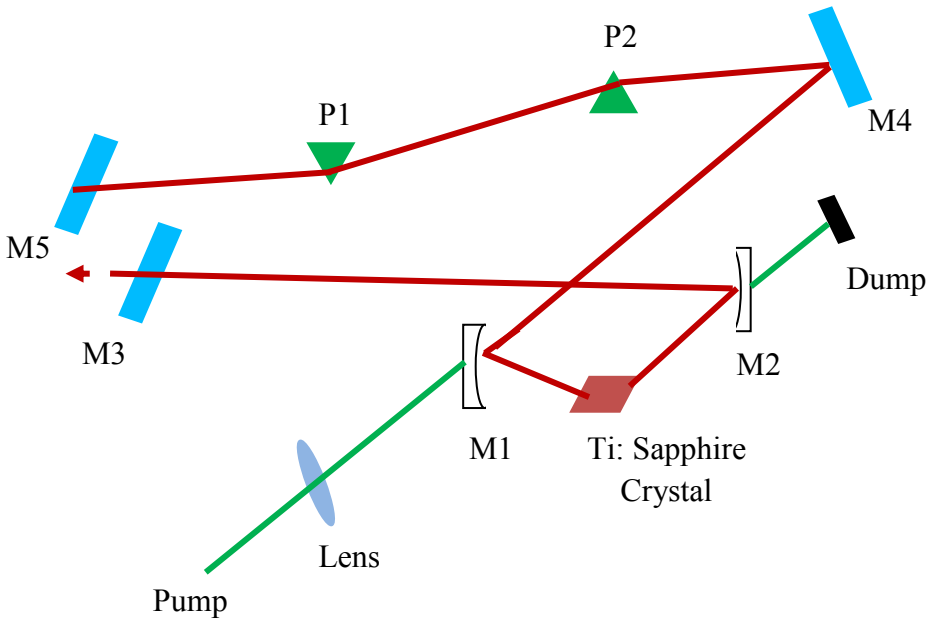

Figure 6 Schematic demonstration of the KM oscillator

4.1.3 Evolution V

Evolution is a Q-switched Nd:YAG laser (Spectra Physics, Merlin) at a repetition rate 1 kHz, output power 10 W emitting at 532 nm wavelength with ~10 ns pulse duration. The gain medium and pump lasers are enclosed inside the laser head and co-located in a directly water cooled resonant cavity. The evolution is used to pump the spitfire.

4.1.4 Spitfire (Regenerative amplifier)

The regenerative amplifier technique is used to amplify femtosecond pulses. In our system in Fig 7, it is used to amplify a seed pulse (KM Oscillator) that generates

thousands of pulses with repetition rate around 80 MHz. However, the amplifier is pumped by evolution that has repetition rate of several kHz. Thus only small part of the pulses from the oscillator is allowed to be amplified. The seed pulse will be inside the cavity when the pump pulse passes through the crystal. When the gain is saturated, the amplified pulses are let out of the cavity. For this reason a fast optical switch that has a response time in the nanosecond range is required. Our Spitfire contains three main parts, stretcher, regenerative cavity and compressor. The seed pulses are expanded in a gain stretcher during the time. A Photodiode that is placed behind one of the cavity mirrors helps one to monitor trace of the femtosecond pulses on the oscilloscope. The Pockels cell changes the refractive index of the material under the applied electric field. So the linearly polarized pulse is generated. The amplifier is pumped by evolution at a repetition rate 1 kHz. The output of the amplifier ~800 mW is a train of the pulses having repetition rate 1 kHz, pulse energy 0.8 μJ and pulse duration is 50 fs [**10**], [**20**].

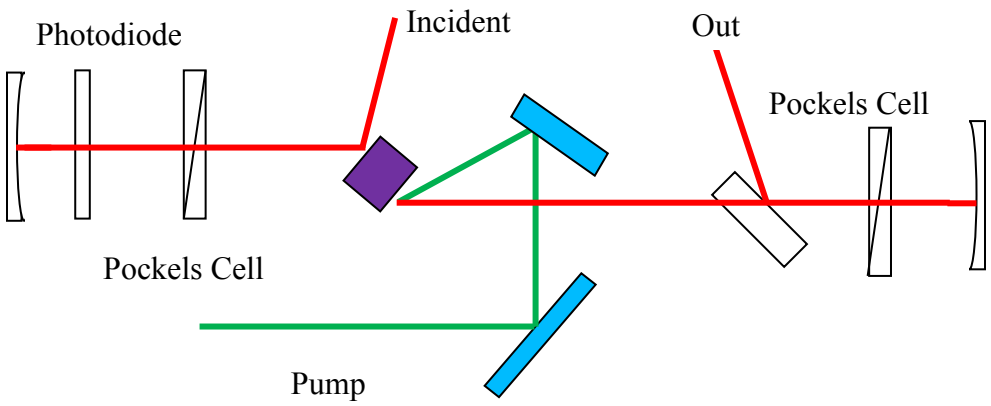

Figure 7 Schematic of Regenerative Cavity

4.2 Pulse Measurement

4.2.1 Frequency Resolved Optical Gating (FROG) – GRENOUILLE

Frequency resolved optical gating (FROG) helps researchers characterize the pulses in the temporal domain. FROG has the ability to measure femtosecond pulse's intensity vs. time [**23**]. The FROG setup shown in Fig. 8 consists of an auto-correlation and a spectrometer's setup. Autocorrelation separate a laser pulse in two and delayed one pulse with respect the other and focusing and recombining them on the nonelinear medium (Second Harmonic Crystal). The SHG crystal produces twice the frequency of the input laser [**23**] and the spectrometer determines the shape and the phase of the laser pulse. The FROG is updated by Trebino et al. They replaced the beam splitter, delay line and beam combining optics with Fresnel biprism [**20**].

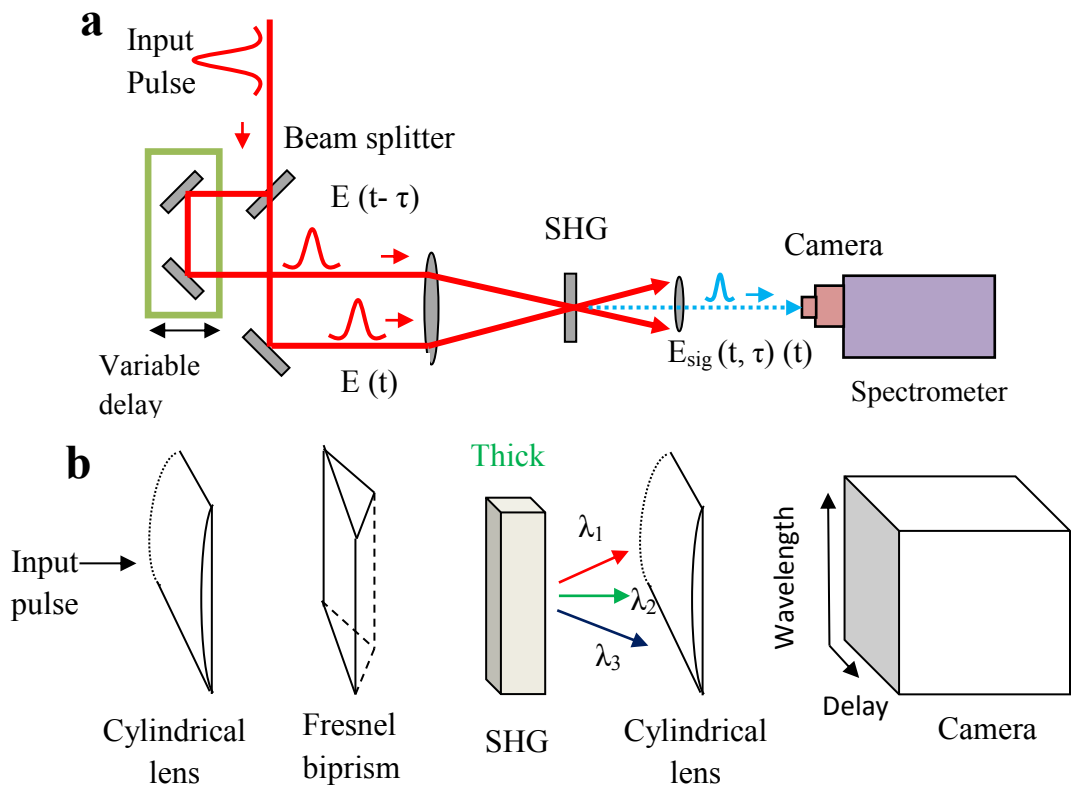

Figure 8 (a) Optical scheme of SHG FROG. (b) GRENOUILLE is the simplest version of the FROG.

Grenouille is a combination of two cylindrical lenses, Fresnel biprism, SHG crystal. The first lens focuses the beam in to SHG crystal, the Fresnel biprism splits the beam, and delays the beam one another, and the second lens focuses the beam in to CCD camera. In Fig.9 show the results of the pulse shape and duration taken from the Grenouille (8-20, Swamp Optic) [**20**].

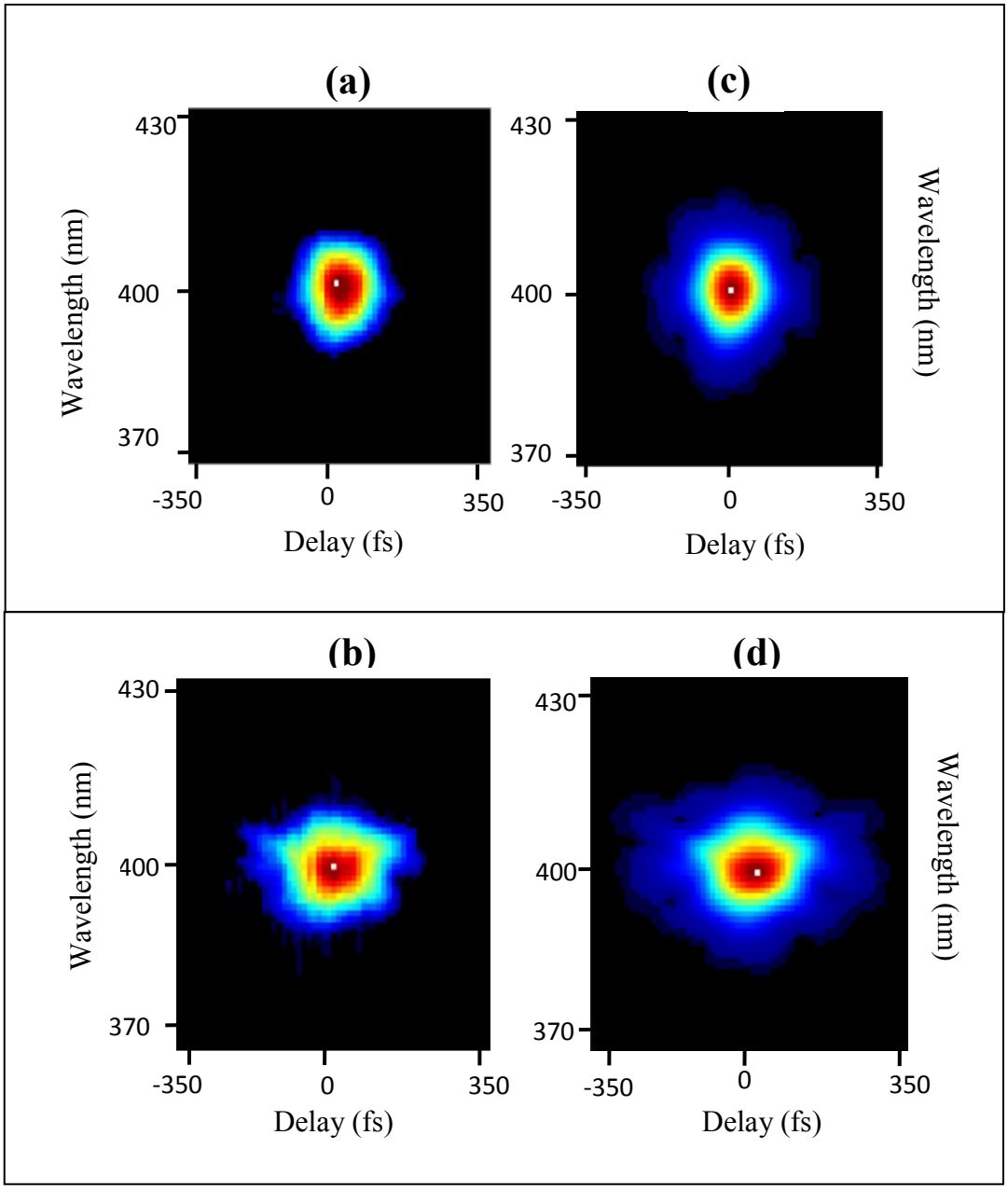

Figure 9 (a) Images of femtosecond pulse taken from GRENOUILLE. (a) Compressed pulse at 52 fs. (b) Stretched at 81 fs. (c, d) Retrieved images are from compressed pulse and the stretched pulse, respectively.

4.3 Optical Setup

In our setup, we focused light from a 1 kHz Ti:Sapphire laser system that produces 50 fs duration pulses with pulse energy of 0.5 mJ into a 1 mm thickness gas jet filled with low pressure argon. The Fig. 14, which is general setup of experiment, is shown on page 27. Before the beam reaches the gas jet, the beam hits the SLM. In our experiment, the SLM (Hamamatsu LCOS-SLM X10468-02) was used, which is suitable to have femtosecond radiation in our setup since the SLM is able to withstand intensities up to $I \approx 10^{11}\ {}^{\mathrm{W}}/_{\mathrm{cm}^2}$ [**24**]. Also it was designed to work efficiently within a wavelength range of 750 nm to 850 nm. The phase modulation of the SLM was produced 2π radians of phase modulation for 800 nm wavelength according to factory calibration [**24**]. In Fig. 10 gives the configuration of the LCOS-SLM. It is made of a glass substrate, an alignment films, a liquid crystal layer, a dielectric mirror and a silicon substrate. Voltage is applied to the silicon substrate, and the phase is modulated by the alignment of the liquid crystal and the dielectric mirror is used to reflect a broad spectrum of light, for example the entire spectrum of the Ti: Sapphire laser. However, for different wavelengths the produced phase shift is different, and in general this effect should be taken into account, i.e. 633 nm He-Ne laser has a larger phase modulation of $\Delta\varphi = 3.2\pi$ [**24**]. The SLM is replaced one of the mirrors to enable manipulation with the wave front of the laser beam that was necessary for other experiments that are not part of this work. In the present work a constant voltage was provided on all pixels of the SLM, corresponding to a constant phase shift across the beam, which did not affect physical mechanisms described in this project.

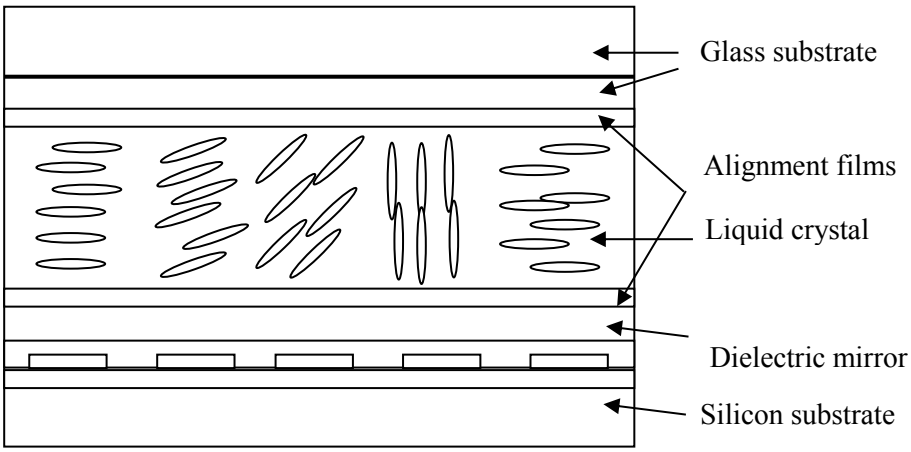

Figure 10 Configuration of LCOS-SLM

An important tool in our setup is an XUV McPherson Monochromator (model 248/310G) that is designed to cover wavelength region from 1 nm to 300 nm. The McPherson Monochromator (model 248/310G) permits the user to adjust the entrance slit, exit slit and grating mount to accommodate gratings whose radius of curvature vary slightly from nominal radius (998.8 mm or 39.323 inches). The McPherson Monochromator is related to actual wavelength by a relationship in Eq. 22 that is plotted in Fig. 11:

$$\boldsymbol{\lambda = d\left[\sin\alpha_i - \sin\left(\frac{\pi}{2} - \sin^{-1}\left(L/(2R_R)\right)\right)\right]} \quad (22)$$

where λ is the wavelength in nanometer, d is the grating function $\left(\frac{1}{133.6}\ mm\right)$, $\alpha_i = 87.6$ degree is the incident angle, L is the counter reading in inch, $R_R = {}^{R_G}/_{2}$ is the radius of the Rowland circle, R_G is the grating radius $R_G = 998.8$ mm.

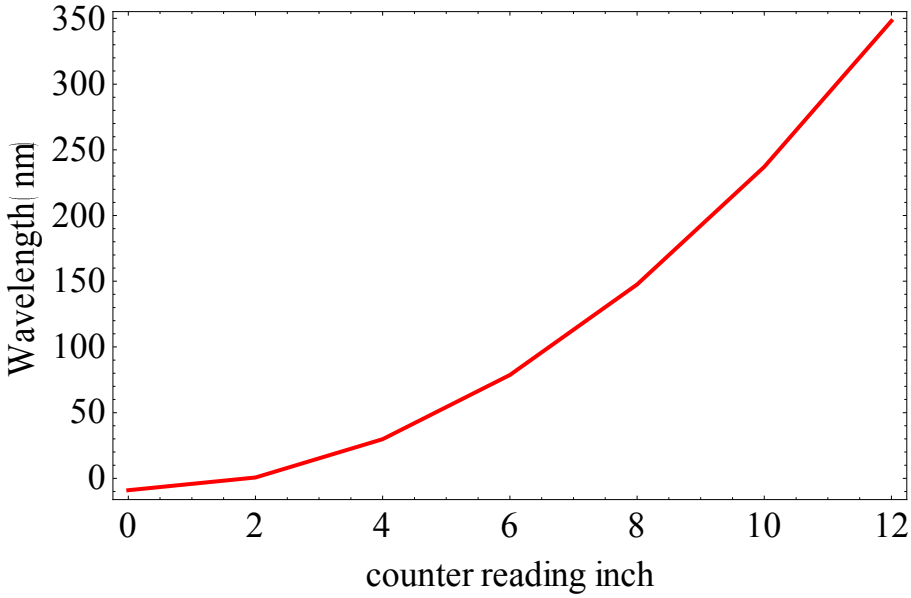

Figure 11 A typical wavelength calibration charts for the distance reading in terms of inches along the Rowland circle

4.4 Micro-channel plate (MCP) and Charge-coupled device (CCD)

An electronic camera (CCD) has been used to measure the duration of single isolated attosecond pulses. An attosecond camera converts temporal information into momentum information. The momentum of electrons can be measured using the well-developed TOF spectrometer (Time of Flight) techniques. The electronic camera works to convert light images to electronic signal. The electron images are then processed by applying 2.5 kV voltage to the micro-channel plate (MCP). MCP is usually used in detectors for electrons, ions, and high-energy photons (UV to x-ray). An MCP looks like the round thin glass plate, with a diameter of 40 mm and thickness of 0.5 mm. It is made by fusing several millions of thin glass tubes together. When an incident photon of light hits the front face of the MCP, it frees electrons. The freed electrons are gained acceleration inside the tiny channels of the MCP applying voltage difference between

the front and the back surfaces of the plate. The freed electrons are hit by the wall of the channel and knock out more electrons, that process is occurred approximately 12 times. As a result, for one incident particle, $\sim 10^3$ electrons can be released from the rear surface. When a pulsed voltage is applied on the MCP, the gain can be turned on and off very rapidly, which serves as a shutter Fig. 12.

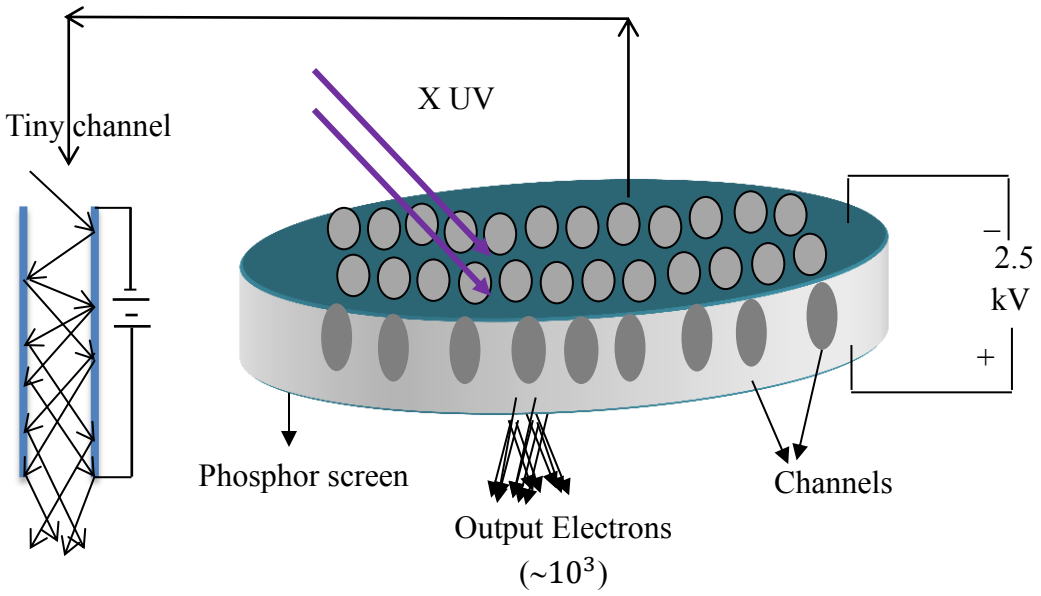

Figure 12 Schematic of a micro-channel plate (MCP)

The main component of a MCP is that it includes a photocathode, a focusing lens, a deflection plate, and a phosphor screen. The electron optic lens images the slit to the phosphor screen, which can be recorded by a CCD camera. Then the computer screen connected by the CCD camera brings us the harmonic picture for our experiment. Also the MCP and the CCD can be scanned along the Rowland circle to catch different XUV radiation. In Fig. 13, the XUV radiation comes through to grating that makes

$\theta = 2$ degree angle with the Rowland circle. The grating then disperses the XUV radiation to different odd harmonics on the Rowland circle. Then MCP (Micro-channel plate), similar to electron multiplier, detects the electrons or ions. Finally imaged electrons by MCP are transmitted to the lens where images are dropped on the CCD camera that it magnifies and centers the electrons on the computer screen [**10**].

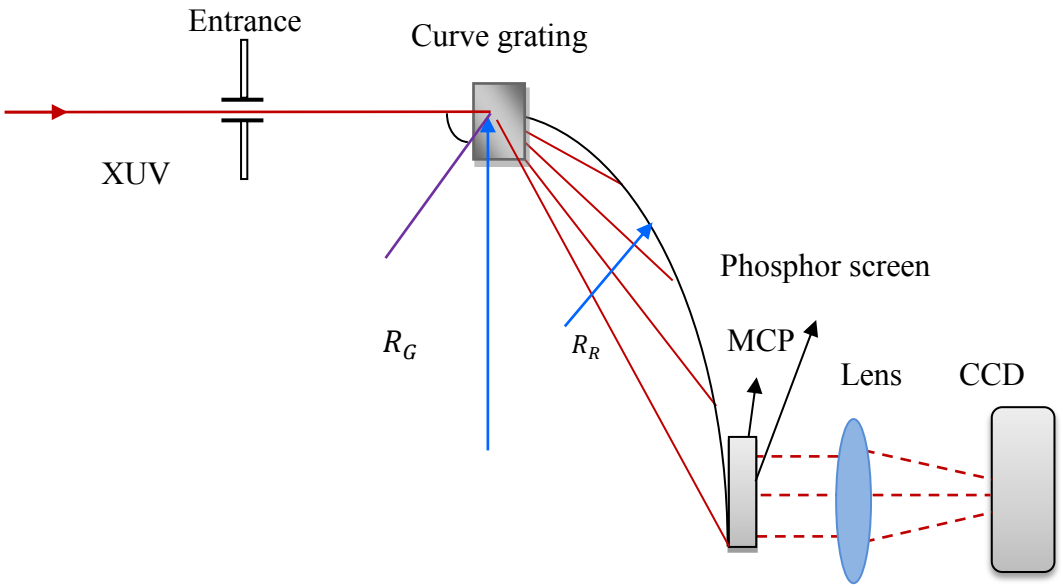

Figure 13 Schematic of the McPherson Monochromator

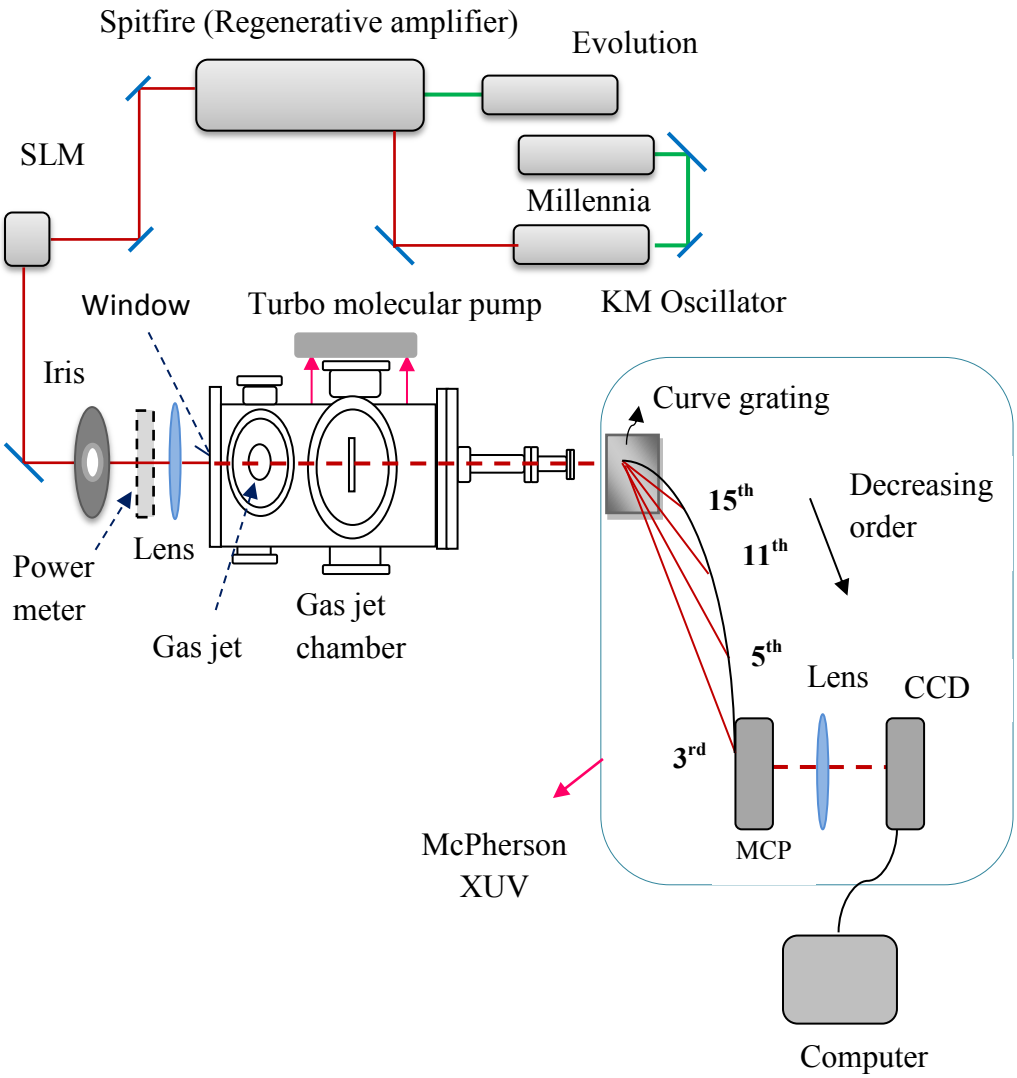

Figure 14 Schematic of the setup for HH generation

We need low vacuum ($\sim 10^{-6}$ mbar) in the chambers then we use 6 pumps, two of them are backing pumps to reach 10^{-3} mbar and four turbo molecular pumps to reach 10^{-6} mbar. In the first pumping stage where HHG is originated the pressure is around 10^{-3} mbar in the chamber. In the second pumping stage where the McPherson spectrometer is located the pressure is around 10^{-6} mbar. We need such a pressure since

the MCP channel would be oxidized in high pressure (low vacuum) then MCP would be damaged, also the XUV light is mostly absorbed in air so XUV required high vacuum (low pressure $\sim 10^{-6}$ mbar) for transmission [**25**] , [**26**].

4.5 Gas Jet

Noble gases are usually used as the detection gas since they have the large ionization potential. When the femtosecond pulses are focused on the atomic gas jet, gas jet behaves as a photocathode. Then the bound electrons confined by Coulomb potential in the gas atoms can leave the gas jet as the XUV photons in Fig. 15. The gas target is located in the chamber vacuumed ($2.5x10^{-3}$ mbar). Due to the low photon flux of the attosecond pulses, the challenge is to have a high length-pressure product to absorb enough XUV photons [**10**].

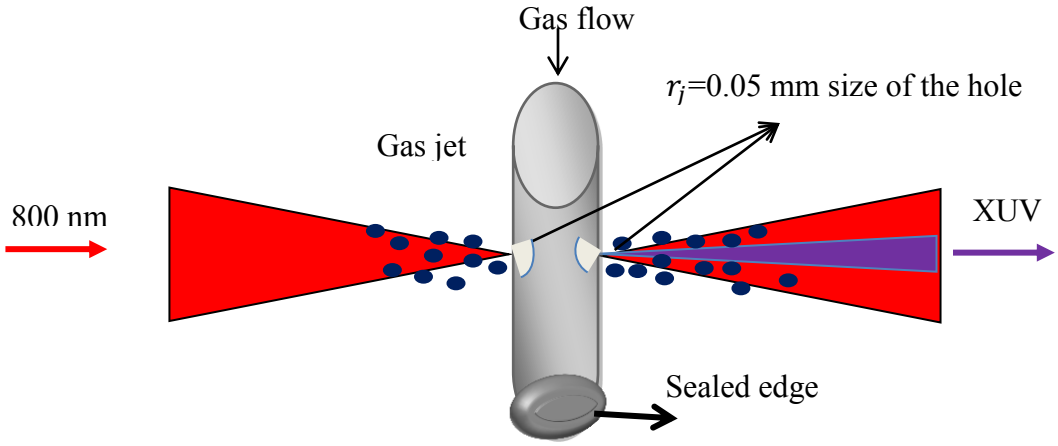

Figure 15 Schematic of the gas jet

Moreover, we calculate the pressure on the gas jet as following way:

Conservation of mass is given:

$$\boldsymbol{\rho_c F_c = 2\pi r_j^2 V_j \rho_j} \quad (23)$$

Where $F_c = 2900$ cm^3/s is pumping rate of chamber, ρ_c is density of gas in the chamber, r_j is the radius of hole on the gas jet, $V_j = \sqrt{\frac{\gamma R T_j}{\mu}} = 380\ m/s$ is velocity of the gas, and ρ_j is the density of the gas in the gas jet, μ is the molar mass, $\gamma = \frac{c_p}{c_v} = 1.66$ is the constant for a monoatomic gas . Then pressure on the jet is given:

$$\boldsymbol{P_j = \frac{\rho_j}{\mu} R T_j = \frac{\rho_c F_c R T_j}{\mu 2\pi r_j^2 V_j}} \quad (24)$$

where $\rho_c = 2.9 \times 10^{-9}$ gr/cm^3, R is the molar gas constant, T is the room temperature. Then we find the pressure on the gas jet is around $P_j = 1.22$ mbar.

4.6 Mixture of Gases

In the experiment, we try to obtain spectrum from mixture of gases. Ne-H_2 and Ne-Ar gases were mixed for different pressure. The setup is given in Fig. 16. Before mixing the gases, the mixture bottle was completely pumped then the experiment was run. The volume of the mixture bottle is around $V = \pi r^2 L$ cm^3 $= 376$ cm^3.

An important part of this experiment is that two gases with different ionization potentials are mixed. These mixtures are Ar- Ne, and H_2-Ne mixtures. The harmonics from Ar and H_2 gases increase the harmonics from Ne. This process is called Dramatic enhancement (DE) [**27**]**.** As a result, harmonics are enhanced and extended by many

orders compared the only Ar or H_2 gas is used. Since there is a large difference in their ionization potentials, first XUV harmonics comes from Ar or H_2 gases. Then the first XUV harmonics boost the harmonic generation to higher orders from Ne atoms.

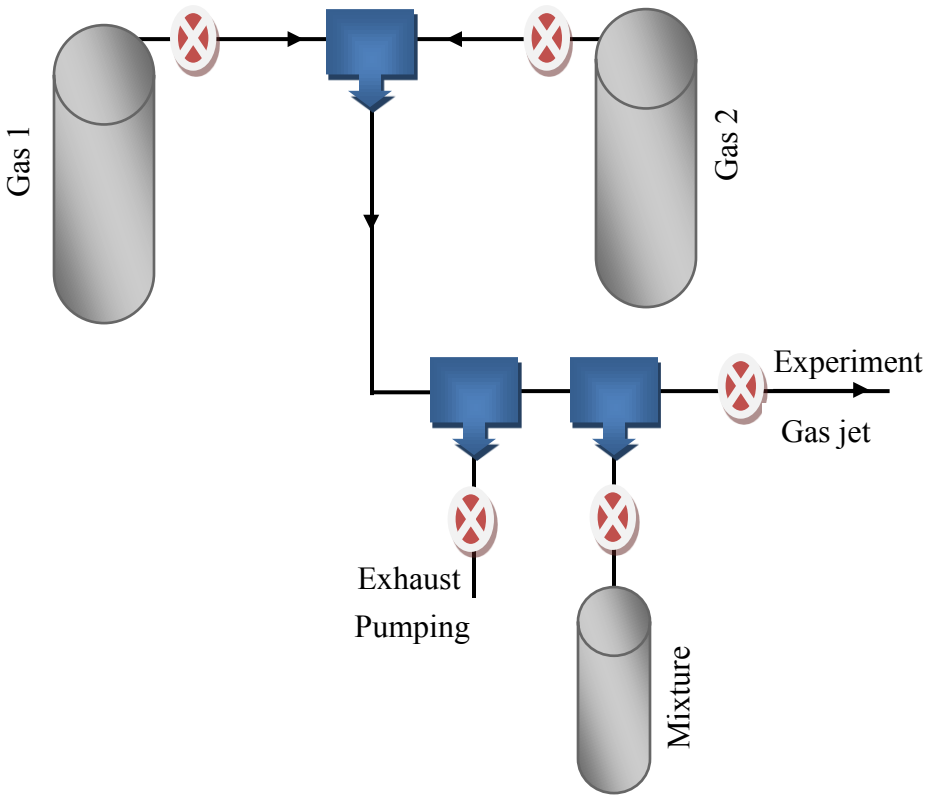

Figure 16 Schematic of the Mixture of Gas Experiment

4.7 Determination of the Beam Size and Intensity

In laser physics, laser beams can be often described in the form of a Gaussian beam. The radial intensity distribution of the Gaussian beam can be written as

$$\mathbf{I(r) = I_0 e^{-2r^2/r_0^2}} \tag{25}$$

To determine the radius of the beam (r_0) one can use an aperture and measure the power of the beam limited by this aperture set to different sizes in Fig. 17. Beam power passing through a circle with a radius r is:

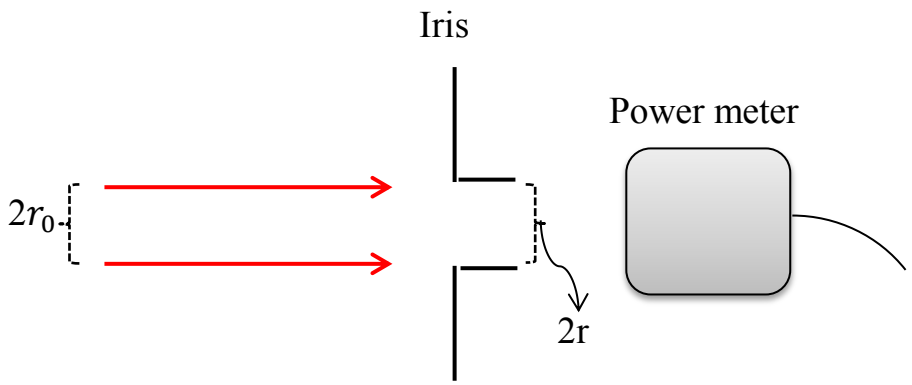

Figure 17 Schematic of the beam size calculation through an iris.

$$\mathbf{P(r) = P_0\left[1 - e^{-2r^2/r_0^2}\right]} \tag{26}$$

where $P_0 = \frac{1}{2}\pi I_0 r_0^2$ is the total power of the beam, r_0 is the beam radius; at $r = r_0$ the intensity of the beam drops to $1/e^2$. The Eq. 25 can be resolved regarding r_0, and we get

$$\boldsymbol{r_0 = \sqrt{\frac{2r^2}{-\log\left(1-\frac{P}{P_0}\right)}}} \tag{27}$$

In calculating the beam radius, we use an iris to block a part of the beam, Fig. 17. We change the radius of the iris in small steps from 0 to 3.5 mm. Then, we measure the power for a set of values of r. When the iris radius is 0 mm, the beam is completely blocked, but if it is >3.5 mm almost the whole beam goes through the iris. Total average power of the beam when the iris is completely open is around 400 mW. Calculating the beam radius according to Eq.26 for each pair $\{r, P(r)\}$ where eight pairs were taken and calculating the average we determine the beam radius $r_0 = 3.33$ mm with error ∓ 0.18 mm.

4.8 Estimates for Kerr – Lens Effect

We produce high harmonic generation (HHG) with a 1 kHz Ti: sapphire laser; the laser pulse at the focusing lens has an energy 0.9 mJ and approximately 50 fs duration. The calculations of intensities and the Kerr-effect estimates for different optical elements are illustrated by Fig. 18.

The intensity in the focused beam is calculated in the following way. The laser intensity of the initial laser pulse is:

$$\mathbf{I_0 = \frac{E_p}{\sqrt{\pi}\tau_0 A} = 1.29x10^{10}\ W/cm^2} \qquad (28)$$

where $E_p = 0.9$ mJ is the pulse energy, τ_0 is the laser pulse duration and $A_{unfoc} = 0.34\ cm^2$ is the area of the unfocused beam.

Then the beam is partially focused at the chamber window and its intensity for the partially focused beam is

$$\mathbf{I_{part}} = \left[\frac{\mathbf{f_k}}{\mathbf{f_k - L_w}}\right]^2 \mathbf{I_0} = \mathbf{1.70x10^{10}\ W/Cm^2} \quad (29)$$

Finally the beam is fully focused at the argon gas by a lens with a focal length $f_k = 40$ cm has intensity

$$\mathbf{I} = \frac{\mathbf{P_{peak}}}{\mathbf{A_{foc}}} = \mathbf{2.72x10^{14}\ W/cm^2} \quad (30)$$

where $P_{peak} = \frac{E_p}{\sqrt{\pi}\tau_0} = 8x10^9$ W and the focused beam area is $A_{foc} = \pi\omega^2 = 2.93x10^{-5}$ cm^2 where $\omega = 3.05x10^{-3}$ cm is the focused beam radius.

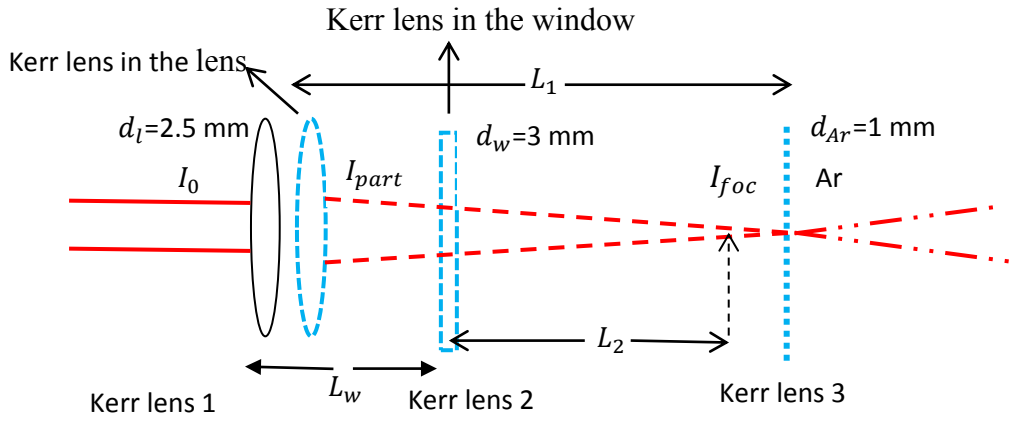

Figure 18 The calculation of the Kerr effect in the propagation of the laser beam through optical elements.

Then we calculate the Kerr effect since the refractive index is affected by the intensity (dynamic Kerr effect), during the high intensity of laser pulse, the nonlinear response play remarkably important role. The refractive index of the medium depends on the laser intensity. It increases from the linear refractive index n_0 to $n(I)$ given as [**10**]:

$$\mathbf{n(I) = n_0 + n_2 I} \tag{31}$$

where n_2 is the nonlinear refractive index.

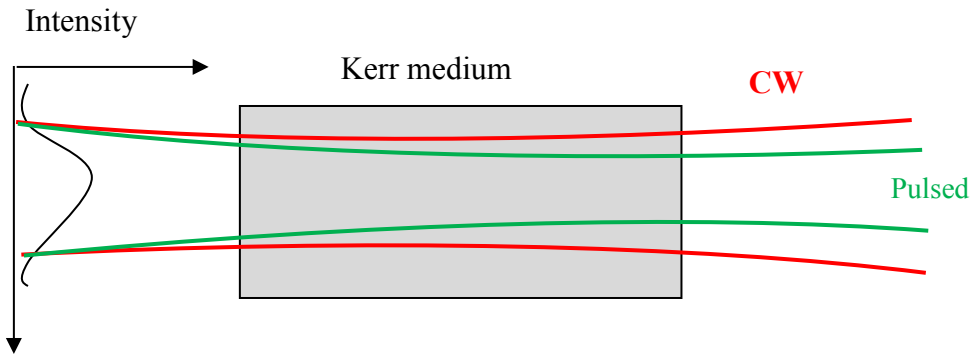

Figure 19 Kerr lens effect on the pulsed (Green) and the continuous light (CW).

The nonlinear refractive index is the maximum at the center of the beam, and gradually decreased to the edge. Laser beam propagates through the nonlinear medium it is focused due to changing nonlinear refractive index. In Fig. 19 is shown that the pulsed laser has strong Kerr lens effect than continuous wave since the pulsed laser has higher intensity than other [**20**].

In the high harmonic generation setup in Fig. 18, the laser beam passes two lenses where the second lens are due to Kerr effect, the window of the vacuum chamber, and the argon gas jet and their refracting indices are also affected by the high intensity of the laser pulse. The lens and the window of the chamber are made of BK7 glass, whose nonlinear refractive index is $n_{2,BK7} = 3.5x10^{-16}\, {cm^2}/{W}$ [**28**].

The Kerr effect for the lens is $\Delta n_{lens}(I) = n(I) - n_0 = 4.52x10^{-6}$, where we used for estimate the linear refractive index of the lens, $n_0 = 1.51$ and the intensity for an unfocused beam $I_0 = 1.29x10^{10}\ {}^{W}/_{Cm^2}$. Thus the Kerr effect for the lens system is small.

The Kerr effect due to chamber window and find $\Delta n_{win}(I) = n(I) - n_0 = 5.94x10^{-6}$ for with window's linear refractive index $n_0 = 1.51$. This effect due to chamber of the window is also negligible in our system.

The Kerr effect due to Argon gas is $\Delta n_{Ar}(I) = n(I) - n_0 = 8.72x10^{-5}$ with nonlinear refractive index of Argon at 1 bar $n_{2,Ar} = 3.2x10^{-19}\ {}^{cm^2}/_{W}$ at 800 nm, $n_{2,Ar} = 3.2x10^{-19}\ {}^{cm^2}/_{W}$ at 800 nm [**28**], [**29**], and at 1 atm $n_{2,Ar} = 9.8x10^{-20}\ {}^{cm^2}/_{W}$ [**30**]. Then we use the value of argon refractive index for 800 nm and intensity at the focus is $2.72x10^{14}\ {}^{W}/_{cm^2}$.

The Kerr effect creates an additional lens which is second lens on Fig. 18 with the nonlinear focal distance

$$\mathbf{f_{nl}} = \frac{\mathbf{r_0^2}}{\mathbf{4n_{2,BK7}d_l I_0}} \tag{32}$$

Also chamber of the window creates Kerr effects and its nonlinear focal length is

$$\mathbf{f_{nlw}} = \frac{\mathbf{r_0^2}}{\mathbf{4n_{2,BK7}d_w I_{part}}} \tag{33}$$

where $d_{lens} = 0.25$ cm is the thickness of the lens. The lens and the window are made of BK7 glass, whose nonlinear refractive index is $n_{2,BK7} = 3.5x10^{-16}\, cm^2/_W$ [**28**]. According to the Eq. 32 and Eq. 33 the nonlinear focal length for the lens and the window are approximately $f_{nl} = 245$ m, and $f_{nlw} = 155\ m$, respectively.

The final position of the focus position of the lens system in Fig. 18 is that

$$\frac{1}{f_k} + \frac{1}{f_{nl}} = \frac{1}{L_1} \tag{34}$$

$$\frac{1}{L_1 - L_w} + \frac{1}{f_{nlw}} = \frac{1}{L_2} \tag{35}$$

Accepting that $\frac{1}{f_{nl}}$ and $\frac{1}{f_{nlw}}$ is much smaller than $\frac{1}{f_k}$ and using power series expansion we get total focus shift

$$\Delta f = -\frac{1}{f_{nl}} f_k^{\,2} - \frac{1}{f_{nlw}} (f_k - L_w)^2 \tag{36}$$

The window is located at a distance of $L_w = 5$ cm away from the focusing lens. The original focal length of the focusing lens is $f_k = 40$ cm. Then the total shift of the focus position is found $\Delta f \approx -0.14\ cm$

4.9 Absorption of XUV Radiation in the Gas Jet Medium

Transmission of HHs in the medium is described by the factor $\propto I = I_0 \exp(-\kappa L)$. The absorption coefficient κ is determined by the absorption cross-section σ_{ph} and the neutral atom density N_{at}

$$\kappa = \sigma_{ph}\ N_{at} \tag{37}$$

where N_{at} is the neutral atom density of argon that is approximately $N_{at}\sim10^{18}\ m^{-3}$ at the $2.5x10^{-3}$ mbar and the absorption cross section's values for argon changes in the interval from $\sigma_{ph} = 3.59x10^{-17}\ cm^2$ to $1.02x10^{-18}\ cm^2$ by harmonic number from 29th harmonic to 11th harmonic, is calculated [**31**]. Using the above values and the thickness $L = 1\ mm$ of the argon gas jet we calculated total absorption for three values of the gas pressure P=10,50 and 100 mbar in the HHG region for several harmonics as shown in Fig. 20. The jumps on the Fig. 20 are due to M_1 edge of the absorption at the wavelength around 42 nm (28 eV). That means transition from 3s level to higher level. Absorption dominates lower harmonics at relatively high gas pressures.

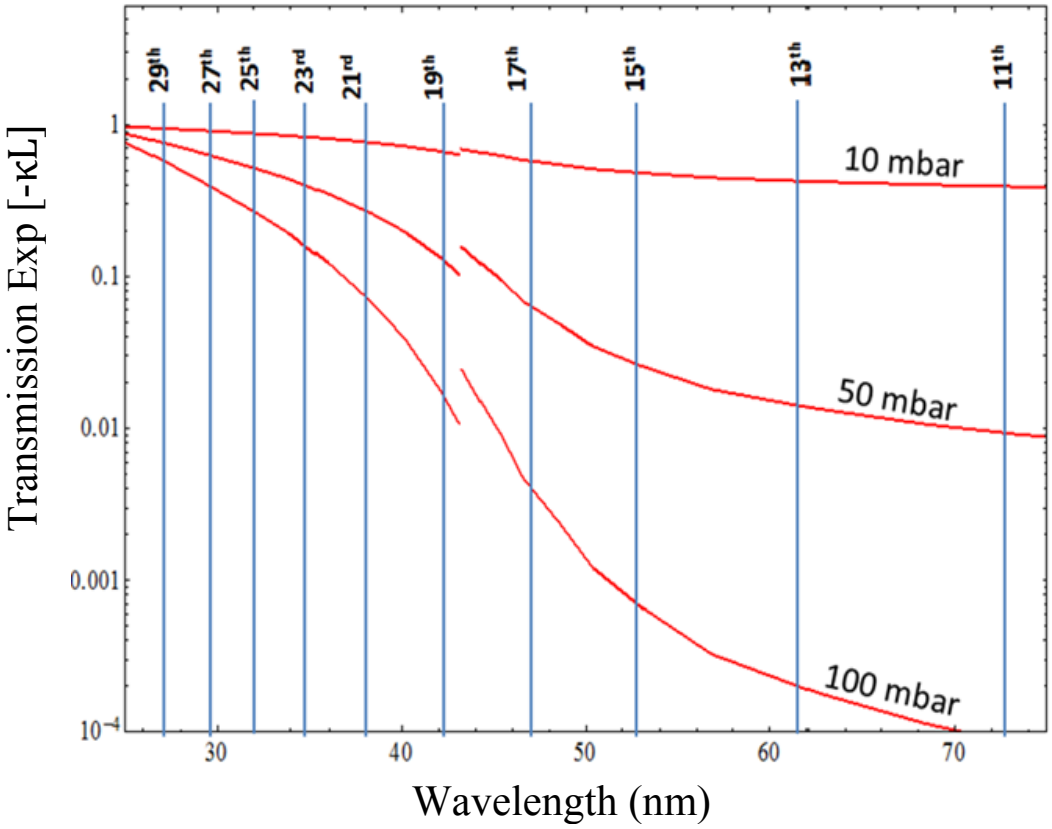

Figure 20 Transmission ($e^{-\kappa L}$) for several harmonics

4.10 Phase Relations in HHG

There are several approaches to get XUV pulse energy in order to reach attosecond pulse duration. The fields that are emitted by the gas atoms in the propagation direction are in the same phase and if they constructive each other so they are said in phase.

Phase matching between the fundamental wave and the generated high harmonic is important for efficient HHG. In this nonlinear process, phase matching depends on both the intensity of the electromagnetic radiation and the order of the nonlinear process. HHG is usually realized in a gas medium by focusing the initial laser beam. Therefore,

the degree of focusing and the dispersion of the medium strongly affect the nonlinear interaction process. The degree of focusing determines the highest intensity that is reached and the rate at which the phase changes near the focus due to the Gouy phase change [**32**]. The dispersion of the refractive index of the medium results in different phase velocities for waves with different frequencies, and causes a phase mismatching [**33**].

The coherence length is the propagation distance from an initial wave to a XUV wave where it maintains specified degree of coherence.

$$L_c \approx \pi / |\mathbf{\Delta k}| \tag{38}$$

where Δk is the wave vector mismatch. The total accumulated phase difference in the medium is proportional to Δk and the propagation length (L) in the medium [**34**] .

In high-harmonic generation, the gas medium under high laser intensity is turned into mixture of neutral atoms and plasma since the ionization of the gas is unavoidable. To calculate phase relations in the HHG, the phase mismatch of the harmonic and the driving infrared field will be considered [**34**]. The phase mismatch can be presented as a sum of four terms: dispersion in the neutral gas $\mathbf{\Delta k_q^g\ cm^{-1}}$, dispersion in the generated plasma $\mathbf{\Delta k_q^p\ cm^{-1}}$, the variation of the dipole phase $\mathbf{\Delta k_q^d\ cm^{-1}}$ and the phase change occurring during focusing of the fundamental Gaussian beam (Gouy phase) $\mathbf{\Delta k_q^f\ cm^{-1}}$:

$$\mathbf{\Delta k_q = \Delta k_q^g + \Delta k_q^p + \Delta k_q^d + \Delta k_q^f} \tag{39}$$

The first term is related to the difference between the refractive indices of the gas for the fundamental radiation and the higher harmonic. If n_q is the refractive index of q^{th} harmonic, then

$$\Delta k_q^g = (n_q - n_1) \frac{q\,\omega_0}{c} \qquad (40)$$

where the c is the speed of light and ω_0 is the fundamental frequency corresponding to the wavelength of the pump beam of 800 nm. The refractive index for the wavelength range of high harmonics from 11^{th} to 65^{th} is shown in Fig.21 [**35**].

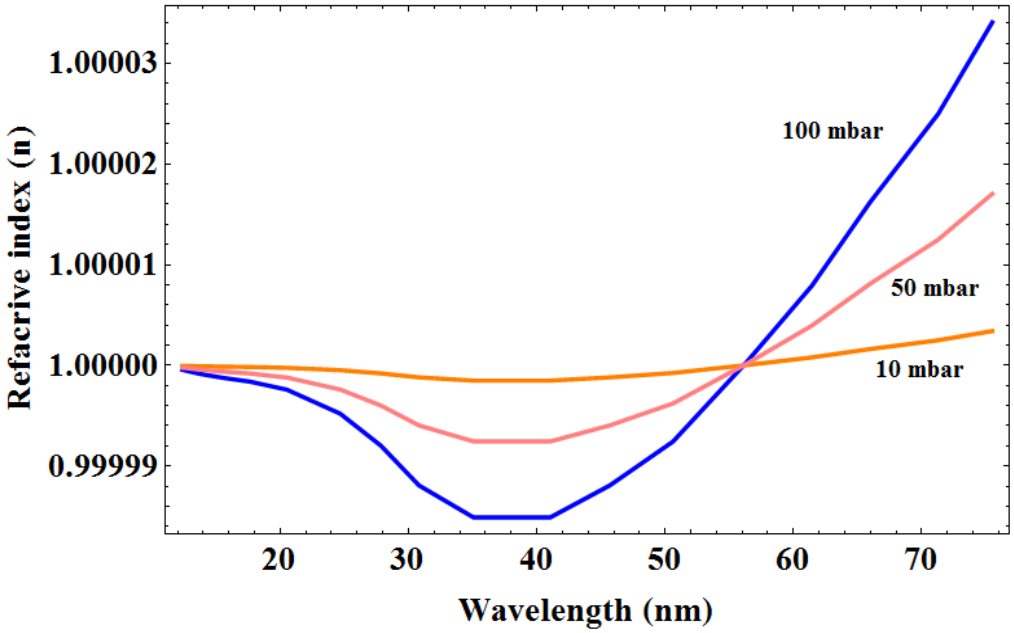

Figure 21 Argon's refractive index for the wavelength interval corresponding to harmonics from 11th to 65th

The refractive index for argon at the 800 nm is $n_1 = 1.00027962$ [**36**]. We have calculated the phase mismatch contribution. $\Delta k_q^g\,\mathrm{cm}^{-1}$ in neutral gas for several harmonics as shown in Table 1.

The second phase mismatch contribution in Eq. 38 Δk_q^p is caused by the generated plasma. Ionization is an inherent process in the HHG. This plasma term depends on the difference of the refractive indices for the fundamental and high harmonics radiation due to the free electron density created:

$$\mathbf{\Delta k_q^p = (n_q^p - n_1^p)\frac{q\,\omega_0}{c}} \tag{41}$$

The refractive index of plasma is given by $n_q^p = \sqrt{1 - \frac{\omega_p^2}{q\omega_0}}$, where ω_p is the plasma frequency, $\omega_p = \sqrt{N_e q_e^2 / m_e \epsilon_0}$ is the plasma frequency, N_e is the density of charges (their number per unit volume), q_e and m_e are the charge and the mass of a free electron, and ϵ_0 is the permittivity of free space.

The electron density is

$$\mathbf{N_e = N(P1 + 2P2)} \tag{42}$$

$N = (N_A P_{pressure})/V$ is the density of the argon at the pressure of 100 mbar, N_A is the Avogadro number and $V = 22.4\,\mathrm{l} = 0.0224\,m^3$. The quantities the P1 and the P2 are the ionization fractions of singly and doubly ionized ions of Ar subjected to the high-intensity pulses. These fractions can be roughly estimated by using the data of [**15**],

where the ionization of Ar was calculated for 18 fs pulse with a peak intensity of $1.3x10^{15}$ $\mathrm{Wcm^{-2}}$. Taking into account that we have 2.5 times longer pulses for the ionization fractions at the typical value of the intensity in our experiments (it corresponds to the cutoff energy 68 eV for $\mathrm{Ar^{+}}$ and 81 eV for $\mathrm{Ar^{++}}$, respectively), we get P1≈ 0.2 and P2≈ 0.0.

Then for the free electron density we obtain $N_e = 2.6875x10^{23}\ m^{-3}$ and we have calculated Δk_q^p ($\mathrm{cm^{-1}}$) for several harmonics, as is shown in Table 1.

The third term in the above Eq.38 Δk_q^d is caused due to change of the dipole phase induced by the variation of the intensity along the beam in the gas cell. This is given by

$$\Delta \mathbf{k_q^d} = \frac{\partial}{\partial z}\left(\frac{\alpha_q I_{foc}}{1+\left(\frac{z}{z_R}\right)^2}\right) \tag{43}$$

where α_q is the harmonic dipole [**37**]; $z_R = \pi\omega_{foc}^2/\lambda_0$ is the Rayleigh length, $\omega_{foc} = 2\lambda_0 f_p/(d_{in}\pi)$ is the beam radius at the focus and λ_0 is the wavelength. $d_{in} = 7$ mm is the iris diameter. Δk_q^d reaches maxima at two different z positions for the long trajectory (typical value $\alpha_q \sim 20 - 25x10^{-14}\ \mathrm{rad\ cm^2/W}$) and for the short trajectory (typical value $\alpha_q \sim 1 - 5x10^{-14}\ \mathrm{rad\ cm^2/W}$). Δk_q^d has a maximum value of -16 to $-20\ \mathrm{cm^{-1}}$ for long trajectory and -1 to $-4\ \mathrm{cm^{-1}}$ for short trajectory at $z = z_R/\sqrt{3}$. $\Delta k_q^d\ \mathrm{cm^{-1}}$

The phase difference between the long and the short trajectories on a 1 mm for P=100 mbar is about radian. Typical values of Δk_q^d are also shown in Table 1.

The last term in Eq.38 occurring while focusing of the fundamental Gaussian beam is called the Gouy phase shift. It is the phase difference between a focused Gaussian beam and a plane wave. The value of the phase changes from $-\pi/2$ to $\pi/2$ for z is from -∞ to ∞ Δk_q^f cm^{-1}:

$$\boldsymbol{\Delta k_q^f = (q-1)\frac{\partial}{\partial z}\left(\tan^{-1}\frac{z}{z_R}\right)} \qquad (44)$$

It has the maximum value at $z = 0$ and its changes are related to phase variations in the focusing on the fundamental Gaussian beam. We also calculated the $\boldsymbol{\Delta k_q^f}$ (cm^{-1}) for several harmonics in Table 1.

HH number	Δk_q^g cm^{-1}	Δk_q^p cm^{-1}	Δk_q^d cm^{-1}		Δk_q^f cm^{-1}
11^{th}	-217.38	66.29	Long trajectory -16 to -20	Short trajectory -1 to -4	30.06
19^{th}	-656.02	115.14			54.11
29^{th}	-652.82	176.02			84.18

Table 1 Phase mismatch for 11^{th}, 19^{th} and 29^{th} harmonics

As shown from the Tab. 1 the phase mismatch gets higher for the higher harmonics. This happens because the higher harmonic has higher energy. We lost the phase matching in the higher harmonics. The prevailing phase mismatch comes from the neutral gas phase mismatch and it increases for higher order harmonics.

4.11 Kerr Lens Mode-locking

In optics, mode-locking technique is used to generate a laser pulse of light for an extremely short duration, on the order of picoseconds (10^{-12}s) or even few femtoseconds (10^{-15}s). The laser resonator must be synchronized in order to generate a short pulse. The synchronization can be achieved by using an element that periodically modulates the losses in the resonator. We use such a laser, a femtosecond oscillator, which employs a Kerr-lens mode-locking effect. In Fig. 22 a laser resonator with two mirrors is shown. One of them is close to being 100% reflective and it plays the role of end mirror. The other mirror is partially reflective and serves as a coupling mirror to output the laser radiation. When the losses in the resonator are smaller than the gain, a laser pulse can be generated. The laser pulse moves back and forth inside the laser cavity and a part of the pulse goes out of the cavity each time when the pulse is reflected from the coupling mirror, so that the repetition rate of the laser pulse train is $fr = \frac{1}{T}$ Hz [**38**], which is an inverse of the pulse round trip time of the pulse in the resonator $T = \frac{2L}{c}$ s, where *L* is the length of the laser cavity and the *c* is the speed of light.

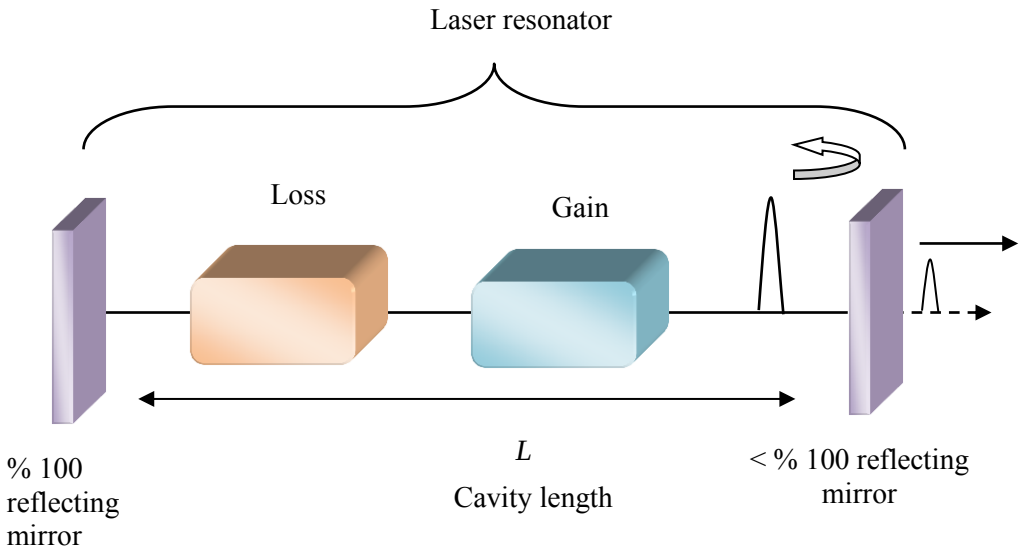

Figure 22 Schematic of a laser resonator with a passive mode-locking.

At the end of the 1980s, Ti: sapphire crystal (Al_2O_3) was discovered as an appropriate laser medium with a sufficient broad gain bandwidth to support the generation of femtosecond pulses. This mode-locking is realized by a Kerr-lens mode-locking mechanism. The refractive index increases according to $\Delta n = n_2 I$ when a higher intensity is passing by the crystal. Even though the KLM mechanism can provide laser pulses with a typical duration of 15-100 fs, it is not self-starting. The switching from the CW operation to a mode-locking regime is achieved by an abrupt perturbation which is created by an initial spike in the intensity. For instance, by mechanically knocking the laser cavity mirror, or as we do in our laser, by clicking of the prisms in the prism pair that is used inside the laser cavity for compensation of the light dispersion.

Light–matter interactions start with the response of the electrons to the light fields. Light is considered as electromagnetic wave under the Maxwell equation. At a

given spatial point, the electric field of a linearly polarized monochromatic laser (also known as continuous wave **(**CW) laser**)** with angular frequency ω can be expressed as

$$\boldsymbol{E(t) = E_0 \cos \omega t} \tag{45}$$

Where E_0 is amplitude of the laser electric field. The magnetic field's amplitude is

$$\boldsymbol{B(t) = B_0 \cos \omega t} \tag{46}$$

The amplitude of the magnetic field is $B_0 = \frac{E_0}{c}$ where c is the speed of light in vacuum.

Mode locking is understood as a linear cavity with a length of L in the z direction, which contains two mirrors and the gain medium. The electric field of the laser can be given as

$$\boldsymbol{E(z') = E(z)e^{-ikz}} \tag{47}$$

In one laser cycle, the electric field repeats itself with certain frequencies $\omega_q = q\omega_0$ where q is integer number and ω_0 is given depending of period of the one laser cycle T

$$\boldsymbol{\omega_0 = 2\pi f_0 = \frac{2\pi}{T}} \tag{48}$$

Electric field having these kind of frequency is called the longitudinal modes. Electric field after the cavity takes form $E_q = E_0 e^{(iq\omega_0 t + \varphi_q)}$. Basicly, assuming the electric fields of all the modes are identical $E_q = E_0$ and if we reach the phase of all modes to be the same, $\varphi_q = \varphi_0$ then we can have mode-locked laser [**10**].

There is a limit for the laser peak power not the damage the material due to high intensity. The critical peak power given as:

$$\boldsymbol{P_{Critical} = \pi(0.61)^2 \frac{\lambda^2}{8(n_0 n_2)}} \quad (49)$$

For our system, we have 800 nm laser light, $n_0 = 1.76\ \frac{cm^2}{W}$ and $n_2 = 2.9x10^{-16}\ \frac{cm^2}{W}$ are the linear and the nonlinear refractive index of the titanium sapphire, respectively. Thus the critical power can be determined according to Eq. 47 $P_{Critical} = 1.83$ MW. Then the laser intensity will be lower if Kerr effect is not enough to distort the properties of the laser pulse. Moreover, large power damages the optics and gain materials [**10**].

5 EXPERIMENTAL RESULTS

The nonlinear interaction between the laser light and the gas atoms produces high harmonics. Photon generation is explained by three step model in the previous chapter. In the experiment, Ti:sapphire laser with a pulse width 50 fs and the central wavelength of 800 nm was focused in the 1 mm gas jet using a 40 cm focal length lens. The laser passes inside the jet while making two holes across the jet that the holes size is small enough to transmit the laser mode. If the pressure on the chamber where the gas jet is located is higher than 10^{-3} mbar , the large number of generated photons is reabsorbed and HHG efficiency would be decreased. For this reason, we need to pump our system. The gas jet was separately included Argon, Hydrogen, Neon, and Mixture Ne-H_2, and Mixture Ne-Ar gases, respectively. The laser intensity at the focus is around $2.72\text{x}10^{14}\ {}^{\text{W}}/_{\text{cm}^2}$. Total pressure of the chamber, where the gas jet is located, is $2.5x10^{-3}$ mbar, also the pressure in the gas jet is 1.22 mbar.

5.1 HHG in Argon

In the experiment, the spectrum obtained for Ar gas. The signals from 11^{th} to 23^{rd} order were observed. In the experiment, a Ti:Sapphire laser with pulse width 52 fs and a central wavelength of 800 nm was focused in the gas cell containing mixed gas Ne and Ar. A 40 cm lens was used to focus the laser beam in the gas cell. The focused intensity is around $\sim 10^{14}\ \frac{\text{W}}{\text{cm}^2}$, and the average power of the spitfire is 930 mW with 1 kHz repetition rate.

We observed the HHs from 21st to 11th for Argon gas. In Fig. 23 gives the plateau from 21st to 15th harmonic. Then the cutoff energy is appeared on the 23rd harmonic. Also, we estimate the ponderomotive energy for intensity$I = 10^{14}\ \frac{W}{cm^2}$, and it is $U_p = 6.2$ eV, and using the ponderomative energy, the cutoff energy for argon gas is $E_{cutoff} = 35.2$ eV that corresponds to 23rd harmonic.

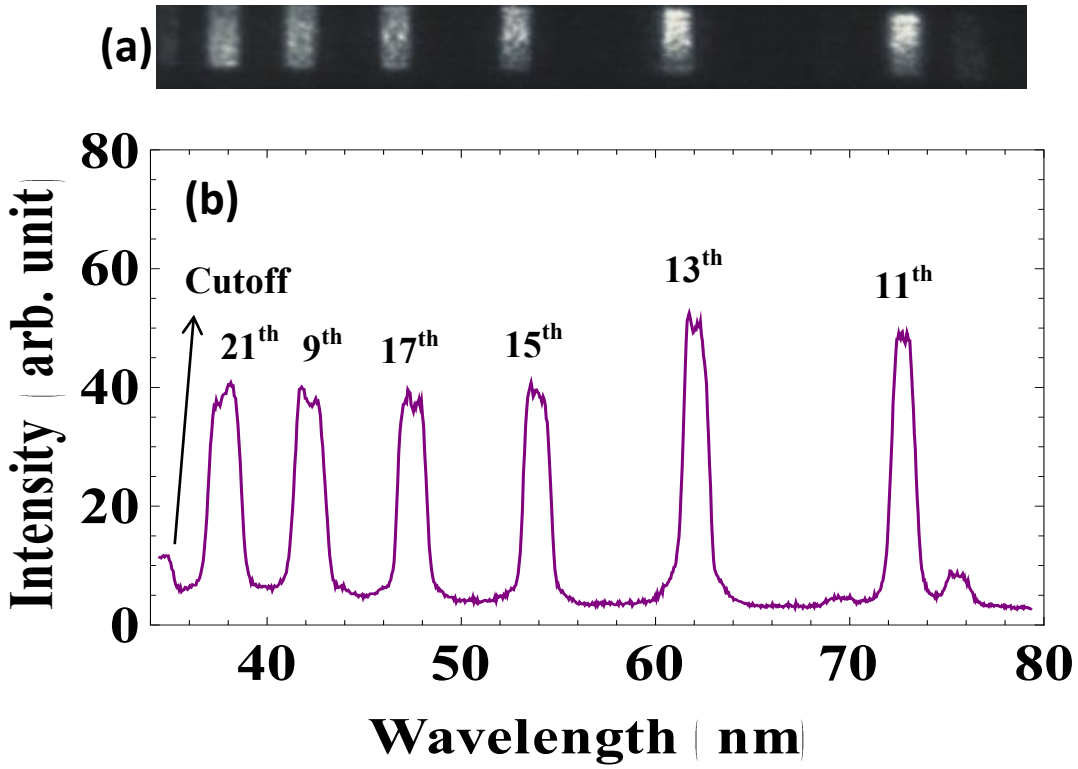

Figure 23 Results for HHG in Ar: (a) Image taken by CCD camera in the experiment with argon, (b) spectrum of HHs in Ar vs. wavelength.

5.2 HHG in Hydrogen Molecule

In the experiment, the spectrum obtained for H_2 gas. The signals from 11th to 21st order were observed. In the experiment, a Ti:Sapphire laser with pulse width 52 fs and a

central wavelength of 800 nm was focused in the gas cell containing mixed gas Ne and Ar. A 40 cm lens was used to focus the laser beam in the gas cell. The focused intensity is around $10^{14}\ \frac{\mathrm{W}}{\mathrm{cm}^2}$, and the average power of the spitfire is 930 mW with 1 kHz repetition rate. The high harmonics from hydrogen molecule is observed up to 19th harmonic, and the cutoff harmonic appears at 21st harmonic in Fig. 24.

The harmonic spectrum using Ne gas was not observed since Ne ionization potential (21.5 eV) [**39**] is high to be ionized for our laser, but we easily determined the harmonics by argon gas with ionization potential 15.6 eV [**39**] and hydrogen gas with ionization potential 13.6 eV [**40**]. The high intensity must be reached to observe HHs with Neon gas. Also the cutoff energy for hydrogen gas is $E_{cutoff} = 33.3$ eV that corresponds to 21rd harmonic.

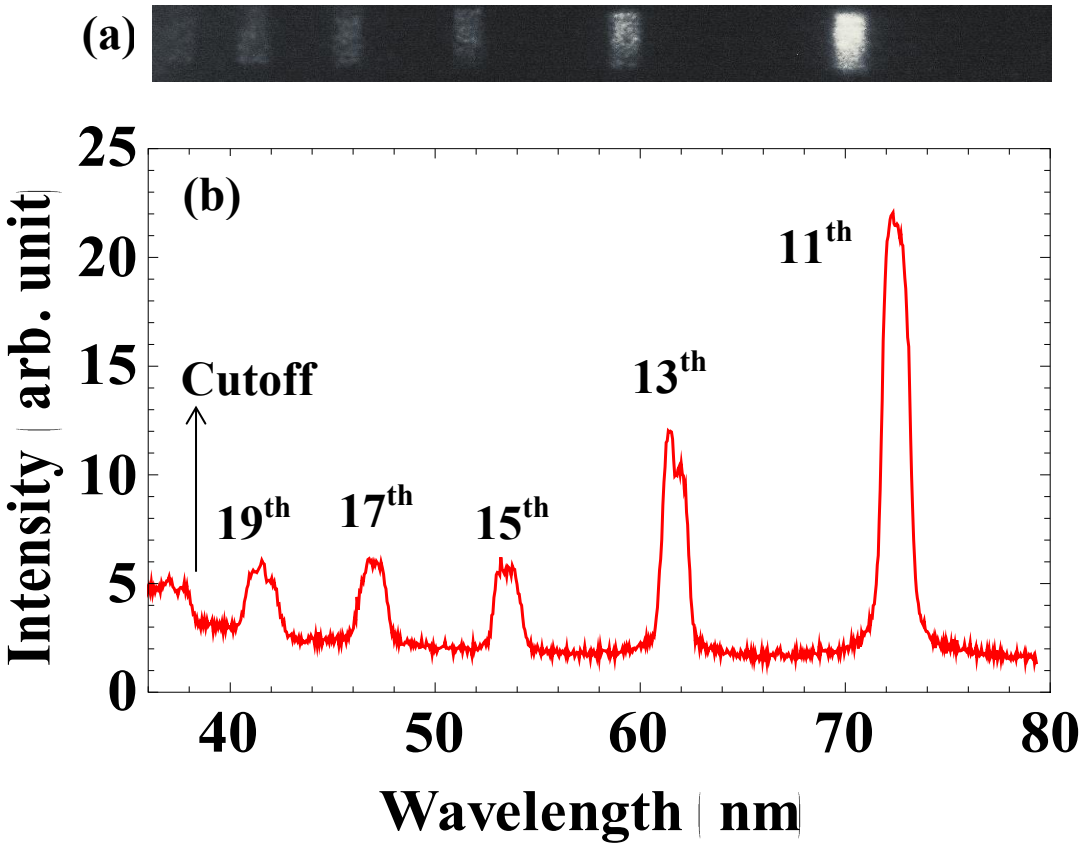

Figure 24 Results for HHG in H_2: (a) Image taken by CCD camera in the experiment with hydrogen, (b) spectrum of HHs in H_2 vs. wavelength.

5.3 Neon and Argon Mixture

We mixed Ne and Ar gases. The pressure of the Ne gas is 1.44 bar and the pressure of the Ar gas is 0.69 bar. In this mixture Ne does not help the enhancement the HHs. The harmonic orders were not observed by using only Ne gas. However, the spectrum obtained with the Ar and Ne- Ar mixture gas gives the same HHs in Fig. 25 [**27**], [**41**]. The harmonic intensity is lower in the mixture gas than only Ar gas spectrum. This may be absorption of the Ne gas.

In an experiment, the Ti:Sapphire laser with pulse width 52 fs and a central wavelength of 800 nm was focused in the gas cell containing mixed gas Ne and Ar. The 40 cm lens was used to focus the laser beam in to the gas cell. The focused intensity is around 10^{14} $\frac{W}{cm^2}$, and the average power of the spitfire is 860 mW with 1 kHz repetition rate.

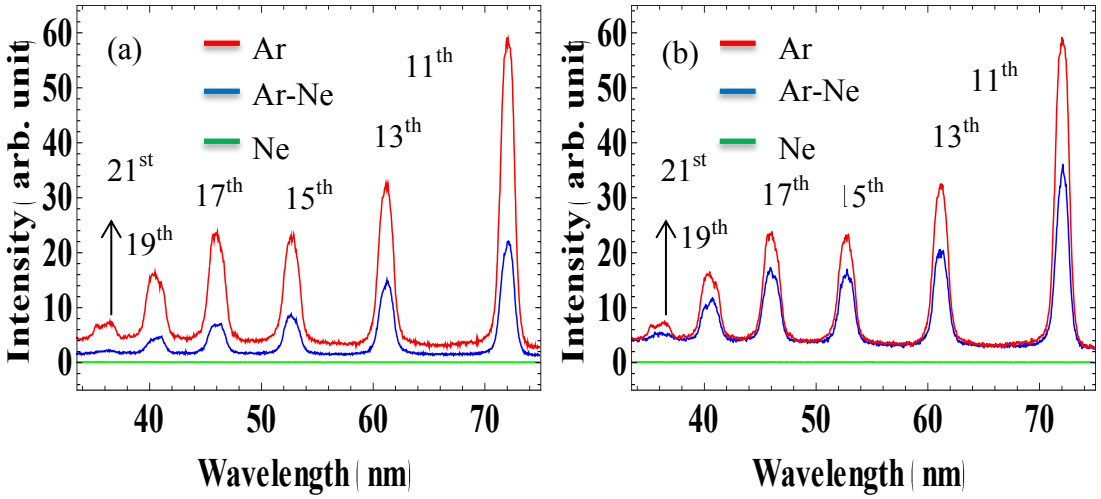

Figure 25 Enhancement of harmonic by mixed gases of Ne and Ar: (a) HH with 1.4 bar Ne, 0.6 bar Ar mixture. (b) HH with 1 bar Ne, 1.7 bar Ar mixture.

5.4 Neon and Hydrogen Mixture

We mixed neon and hydrogen gas for different pressure. In Fig. 26 (a), (b), and (c) show the mixture of gas spectrum, and their pressure values that are 0.6 bar neon with 2 bar hydrogen gas, are 1 bar neon with 1.7 bar hydrogen gas, and 2 bar neon with 0.6 bar hydrogen gas, respectively. Also, In Fig. 26 (d) shows HHs in hydrogen gas for different pressure. In Fig. 26 is Enhancement of harmonic by mixed gases of Neon and Hydrogen gases. Green and red Lines indicate spectra obtained when only Ne and only

H_2 are used, respectively. Blue indicates the spectrum when a mixed gas of Ne and H_2 is used. In Ne and H_2 mixture, we observed remarkably enhancement of the HHs. When the Ne pressure is lower than the H_2, we see the harmonics enhanced in (a), (b) of Fig. 26. However, in (c) of Fig. 26 the Ne pressure is larger than the H_2, the HHs intensity is decreased. Also the HHs intensity is decreased in Fig. 26 (d) when the pressure is decreased. These are because of the fact that in low pressure HHs are more absorbed [**27**], [**41**].

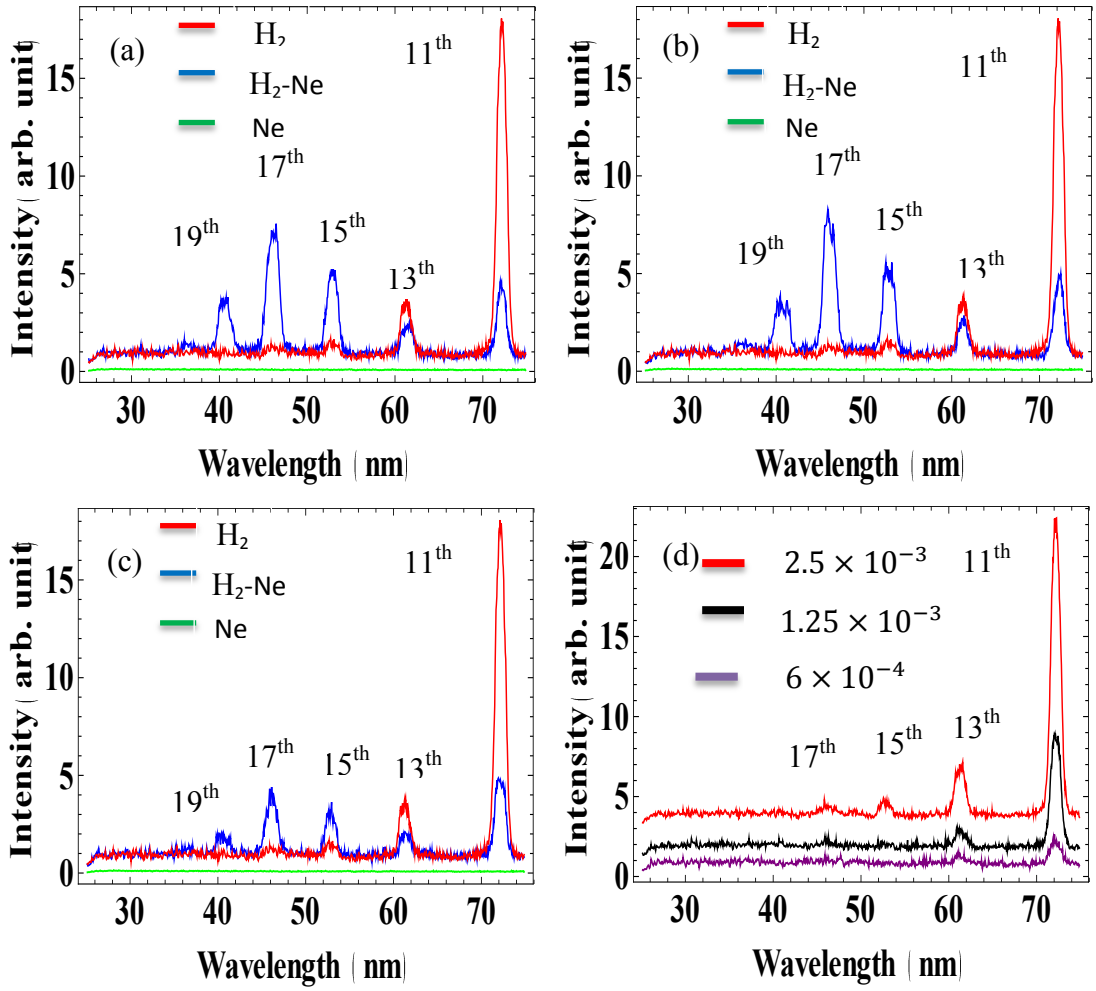

Figure 26 In (a), (b), and (c) Enhancement of harmonic by mixed gases of Ne and H_2. In (d) HHs in H_2 gas for different pressure (mbar).

In an experiment, the Ti:Sapphire laser with pulse width 52 fs and a central wavelength of 800 nm was focused in the gas cell containing mixed gas Ne and Ar. The 40 cm lens was used to focus the laser beam in the gas cell. The focused intensity is around 10^{14} $\frac{W}{cm^2}$, and the average power of the spitfire is 860 mW with 1 kHz repetition rate. For the spectrum obtained using only Ne gas, harmonic orders did not observed and

the spectrum obtained only H_2 gas, 11^{th} to 15 th harmonics are observed. However, the spectrum obtained with the Ne-H_2 mixture gas gives the HHs of 11^{th} to 19^{th}.

6 CONCLUSIONS

Spectra of HHs in the XUV region were observed with a table-top laser system at the 800 nm excitation wavelength. The spectra of HHG from a gas jet filled with argon gas, hydrogen molecule or their mixtures with neon gas have been experimentally investigated. The harmonic spectrum using Ne gas was not observed for the used intensities and gas pressure. However, the spectra of HHs up to 21^{st} order were observed for argon and hydrogen gas when the laser power was 930 mW.

In Ar-Ne mixtures, spectrum does not extend to higher harmonics compared to Ar gas alone. In H_2-Ne mixtures, the cutoff of HHG was extended compared to H_2, namely, HHs were observed up to 19^{th} order for the mixtures, while the spectrum for only H_2 gas extended only up to 15^{th} harmonic. In H_2-Ne mixtures, for improving the conversion efficiency (that is usually in the order of 10^{-5} or 10^{-6}) of the fundamental light into high harmonics in Ne, we use Ne and H_2 gas mixture. We observed up to 20-fold increase in the output of the HHs to higher orders by using moderate laser intensities.

We relate the enhancement mechanism to a more efficient ionization of Ne with addition of H_2. At moderate intensities the ionization of H_2 is relatively easy, leading to HHG in the hydrogen component first. Then the ionization of Ne can be produced via several channels: (1) the generated 11^{th} harmonic leads to a transition from the ground state of Ne to an intermediate state, from which the ionization can be performed with a photon of the third harmonic; (2) the 13th harmonic can resonantly excite from the ground state to a state, from which ionization can be achieved by a single photon of the

fundamental radiation; (3) the tunneling ionization from the excited states has much higher probability than from the ground state. The laser-induced dynamic Stark shift also affects the probabilities of these transitions. We report on the observation of the enhancement effect for different laser intensities and mixing ratios.

REFERENCES

[1] C. B. Madsen, *Molecules in Intense Laser Fields: Studies of Ionization, High-Order Harmonic Generation and Alignment, Ph.D Dissertation, University of Aarhus*., 2010.

[2] C. Cirelli, U. Keller, L. Gallmann, "Attosecond Science: Recent Highlights and Future Trends," *Annual Review of Physical Chemistry*, vol. 63, pp. 447-467, 2012.

[3] M. Drescher, et al., "X-Ray Pulses Approaching the Attosecond Frontier," *Science*, vol. 291, pp. 1923-1927, 2001.

[4] J. Itatani, et al., "Tomographic Imaging of Molecular Orbitals," *Nature*, vol. 432, pp. 867-871, 2004.

[5] R. Velotta, et al., "Interference Effects in High-Order Harmonic Generation with Molecules," *Physical Review A*, vol. 66, 2002.

[6] S.Baker, et al., "Probing Proton Dynamics in Molecules on an Attosecond Time Scale," *Science*, vol. 312, pp. 424-427, 2006.

[7] A. Le, et al., "Theory of High-Order Harmonic Generation from Molecules by Intense Laser Pulses," *Journal of Physics B: Atomic, Molecular and Optical Physics*, vol. 41, pp. 1-10, 2008.

[8] D. J. Griffiths, *Introduction to Electrodynamics , 3rd edition*. New Jersey: Prentice Hall, 1999.

[9] J. T. Verdeyen, *Laser Electronics*. New Jersey: Prentice Hall, 1981.

[10] Z. Chang, *Fundamental of Attosecond Optics*. Florida: CRC Press, 2011.

[11] S. Haessler, et al., "Attosecond Imaging of Molecular Electronic Wavepackets," *Nature Physics*, vol. 6, pp. 200-206, 2010.

[12] M. Murakami, *High Harmonic Generation by Short Laser Pulses: Time-Frequency Behaviour and Applications to Attophysics, Ph.D Dissertation, Louisiana State University*., 2006.

[13] P. B. Corkum, "Plasma Perspective on Strong-Field Multiphoton Ionization," *Physical Review Letters*, vol. 71, pp. 1994-1997, 1993.

[14] K. J. Schafer, K. C. Kulander J. L. Krause, "High-Order Harmonic Generation from Atoms and Ions in the High Intensity Regime," *Physical Review Letters*, vol. 68, pp. 3535-3538, 1992.

[15] E. A. Gibson, et al., "High-Order Harmonic Generation up to 250 eV from Highly Ionized Argon," *Physical Review Letters*, vol. 92, 2004.

[16] K. L. Ishikawa, "High-Harmonic Generation," in *Advances in Solid State Lasers Development and Applications*. Rijeka: InTech, 2010, pp. 439-465.

[17] F. Krausz, P. B. Corkum, "Attosecond Science," *Nature Physics*, vol. 3, pp. 381-387, 2007.

[18] Y. Nabekawa, et al., "Conclusive Evidence of an Attosecond Pulse Train Observed with the Mode-Resolved Autocorrelation Technique," *Physical Review Letters*, vol. 96, 2006.

[19] M. Lewenstein, et al., "Theory of High-Harmonic Generation by Low-Frequency

Laser Fields," *Physical Review A*, vol. 49, pp. 2117-2132, 1994.

[20] M. P. Poudel, *Characterization of Two-Photon Excitation: Coherent Control and Nonlinear Propagation in Transaparent Media, Ph.D Dissertation, Texas A&M University*., 2009.

[21] *Spectra Physics Laser, User Manual*.

[22] *Spectra Physics Laser Millennia, User Manual*.

[23] (2013, January) http://swampoptics.com/tutorials_autocorrelation.htm.

[24] J. Strohaber, et al., "In Situ Tomography of Femtosecond Optical Beams with a Holographic Knife-Edge," *Optics Express*, vol. 19, 2011.

[25] M. Schultze, et al., "State-of-the-Art Attosecond Metrology," *Journal of Electron Spectroscopy and Related Phenomena*, vol. 184, pp. 68-77, 2011.

[26] W. Cao, et al., "Spectral Splitting and Quantum Path Study of High-Harmonic Generation from a Semi-Infinite Gas Cell," *Journal of Physics B: Atomic, Molecular and Optical Physics*, vol. 45, pp. 1-10, 2012.

[27] E.J. Takahashi, et al., "Dramatic Enhancement of High-Order Harmonic Generation," *Physical Review Letters*, vol. 99, 2007.

[28] C. Marceau, et al., "Femtosecond Filament Induced Birefringence in Argon and in Air: Ultrafast Refractive Index Change," *Optics Communications*, vol. 283, pp. 2732–2736, 2009.

[29] P. Béjot, et al., "Ultrafast Gaseous “Half-Wave Plate”," *Optics Express*, vol. 16, pp.

7564-7570, 2008.

[30] Y.-H. Cheng, Y.-H. Chen, H. M. Milchberg, J. K. Wahlstrand, "Optical Nonlinearity in Ar and N2 Near the Ionization Threshold," *Physical Review Letters*, vol. 107, pp. 1-5, 2011.

[31] G. L. Weissler, P. Lee, "Absorption Cross Section of Helium and Argon in the Extreme Ultraviolet," *Physical Review*, vol. 99, pp. 540-543, 1955.

[32] F. Lindner, et al., "Gouy Phase Shift for Few-Cycle Laser Pulses," *Physical Review Letters*, vol. 92, 2004.

[33] K. J. Schafer, K. C. Kulander, A. L'Huillier, "High-Order Harmonic Generation in Xenon at 1064 nm: The Role of Phase Matching," *Physical Review Letters*, vol. 66, pp. 2200-2203, 1991.

[34] T. Balciunas, *Design and Implementation of an XUV-Pump IR-Probe Transient Grating Experiment, Master Thesis, Lund University*., 2009.

[35] J. M. Dahlström, *Light-Matter Interaction on the Attosecond Timescale, Ph.D Dissertation, Lund University*., 2011.

[36] M. J. Weber, *Handbook of Optical Materials*.: CRC Press, 2003.

[37] F. Schapper, et al., "Spatial Fingerprint of Quantum Path Interferences in High Order Harmonic Generation," *Optical Express*, vol. 18, pp. 2987-2994, 2010.

[38] U. Keller, "Recent Developments in Compact Ultrafast Lasers," *Nature*, vol. 424, pp. 831-838, 2003.

[39] R. L. Womer, "Ionization of Hellium, Neon, and Argon," *Physical Review*, vol. 38, pp. 454-456, 1931.

[40] W. Bleakney, "The Ionization Potential of Molecular Hydrogen," *Physical Review*, vol. 40, pp. 496-501, 1932.

[41] K. Midorikawa, "High-Order Harmonic Generation and Attosecond Science," *Japanese Journal of Applied Physics*, vol. 50, pp. 1-12, 2011.